Environmental Science
Processes & Impacts

Biogeochemical and Hydrologic Synergy Control Mercury Fate in an Arid Land River-Reservoir System

Journal:	*Environmental Science: Processes & Impacts*
Manuscript ID	EM-ART-01-2023-000032.R1
Article Type:	Paper

Environmental Significance Statement

Reservoir impoundments of rivers have profound impacts on ecological and biogeochemical processes of contaminants, particularly in arid landscapes. The risk posed by mercury, a metal that bioaccumulates to toxic levels in the form of methylmercury, is exacerbated in reservoirs as a result of toxic methylmercury formation under low oxygen conditions. This study demonstrates that methylmercury accumulates at depth in a reservoir during stratification simultaneous with transformations of particles in the water. Seasonal destratification, driven by river-reservoir hydrology, mobilizes methylmercury in water and on organic-rich particles downstream. These processes affect methylmercury uptake in aquatic food webs and inform management of arid land reservoirs towards the goals of decreasing methylmercury exposure within and downstream of reservoirs.

Biogeochemical and Hydrologic Synergy Control Mercury Fate in an Arid Land River-Reservoir System

Brett A. Poulin[1*], Michael T. Tate[2], Jacob Ogorek[2], Sara E. Breitmeyer[3], Austin K. Baldwin[4], Alysa M. Yoder[4], Reed Harris[5], Jesse Naymik[6], Nick Gastelecutto[6], Charles Hoovestol[6], Christopher Larsen[6], Ralph Myers[6], George R. Aiken[7†], David P. Krabbenhoft[2]

[1]Department of Environmental Toxicology, University of California, Davis, USA

[2]U.S. Geological Survey, Upper Midwest Water Science Center, USA

[3]U.S. Geological Survey, New Jersey Water Science Center, USA

[4]U.S. Geological Survey, Idaho Water Science Center, USA

[5]Reed Harris Environmental Ltd, Toronto, Canada

[6]Idaho Power Company, USA

[7]U.S. Geological Survey, Water Mission Area, USA

*Corresponding author. Tel: +1 530 754 2454. *Email address:* bapoulin@ucdavis.edu

†deseased

Abstract

Reservoirs in arid landscapes provide critical water storage and hydroelectric power but influence the transport and biogeochemical cycling of mercury (Hg). Improved management of reservoirs to mitigate the supply and uptake of bioavailable methylmercury (MeHg) in aquatic food webs will benefit from a mechanistic understanding of inorganic divalent Hg (Hg(II)) and MeHg fate within and downstream of reservoirs. Here, we quantified Hg(II), MeHg, and other pertinent biogeochemical constituents in water (filtered and associated with particles) at high temporal resolution from 2016-2020. This was done (1) at inflow and outflow locations of three successive hydroelectric reservoirs (Snake River, Idaho, Oregon) and (2) vertically and longitudinally within the first reservoir (Brownlee Reservoir). Under spring high flow, upstream inputs of particulate Hg (Hg(II) and MeHg) and filter-passing Hg(II) to Brownlee Reservoir

were governed by total suspended solids and dissolved organic matter, respectively. Under redox stratified conditions in summer, net MeHg formation in the meta- and hypolimnion of Brownlee reservoir yielded elevated filter-passing and particulate MeHg concentrations, the latter exceeding 500 ng g^{-1} on particles. Simultaneously, the organic matter content of particulates increased longitudinally in the reservoir (from 9-29%) and temporally with stratified duration. In late summer and fall, destratification mobilized MeHg from the upgradient metalimnion and the downgradient hypolimnion of Brownlee Reservoir, respectively, resulting in downstream export of elevated filter-passing MeHg and organic-rich particles enriched in MeHg (up to 43% MeHg). We document coupled biogeochemical and hydrologic processes that yield in-reservoir MeHg accumulation and MeHg export in water and particles, which impacts MeHg uptake in aquatic food webs within and downstream of reservoirs.

Introduction

Mercury (Hg) is a global contaminant that impacts both wildlife and human health.[1,2] Emissions of inorganic Hg to the atmosphere from coal combustion and other anthropogenic activities have resulted in a five-fold enrichment of the atmosphere compared to preindustrial levels.[1] Atmospheric Hg is transported regionally and globally and deposited on the landscape by wet deposition of inorganic divalent Hg (Hg(II)) and dry deposition of gaseous elemental Hg (Hg(0)).[3] In aquatic environments, risk associated with exposure of wildlife and humans to Hg (via consumption of fish exceeding the consumption criteria) is ultimately governed by three processes: the formation of methylmercury (MeHg) by anaerobic bacteria and archaea,[4,5] the bioaccumulation of MeHg at the base of the aquatic food web (e.g., phytoplankton),[6,7] and the biomagnification of MeHg in aquatic food webs to toxic levels in fish muscle.[2] Flooding associated with new reservoirs has been well-documented to produce MeHg and increased fish mercury concentrations which can last up to a few decades,[8,9] though the timing and magnitude of the response can vary between systems.[10] Older reservoirs can also exhibit enhanced MeHg formation in anoxic waters[11] and sediments and downstream MeHg export,[12–15] exacerbating

MeHg uptake in proximal aquatic food webs.[12,16,17] Provided the regional and national importance of reservoirs in arid landscapes and projected increases in water stress of North American rivers due to climate drivers,[18] integrated science to support reservoir management to mitigate contaminant fate may be effective to sustain the health of freshwater ecosystems. To this end, an improved understanding of the coupled biogeochemical and hydrologic processes that control Hg(II) and MeHg fate is needed.

Reservoirs can have a disproportionate influence on aquatic Hg cycling due to the unique biogeochemistry and hydrology that arises from the impoundment of rivers. In riverine environments, the transport of particulate and filter-passing Hg(II) is tightly coupled to that of particulate organic matter (POM) and dissolved organic matter (DOM), respectively,[19–23] a result of the co-transport of Hg(II) with organic matter that is often associated with high flow.[19,21,24] In contrast, MeHg in rivers is not solely governed by flow-driven phenomena, as concentrations of filter-passing MeHg are highly variable after accounting for flow and DOM concentration.[21,25] Concentrations of MeHg in riverine surface waters are understood to reflect the culmination of MeHg inputs from tributaries and MeHg contributions from proximal anoxic environments (e.g., riparian pore waters).[26,27] As riverine water enters a reservoir, decreases in water velocities result in sedimentation of POM[28] and some reservoirs thermally stratify, the latter controlled by flow, depth, and operation of reservoir withdraws.[29] These processes have a cascade of biogeochemical consequences that influence Hg(II) and MeHg. First, reservoirs enhance primary productivity[30] which increases POM deposition to deeper waters and sediments and yields shifts in the concentration and composition of DOM.[31–33] Hg(II)-DOM interactions strongly influence the geochemical nature[34–37] and bioavailability of Hg(II) to methylating microbial communities.[38] Second, greater biological oxygen demand fuels the development of hypoxic and anoxic conditions in the metalimnion and hypolimnion of reservoirs that promote Hg(II) methylation to MeHg,[11,15,39] resulting in elevated MeHg concentrations in water (filtered and associated with particles).[40] Microbial metagenomic studies in eutrophic lakes pointed to diverse anaerobic microbial communities possessing

the genes for Hg(II) methylation (*hgcAB*).[4,41] Lastly, MeHg that accumulates in hypoxic and anoxic reservoir waters can partition to particles (e.g., phytoplankton and thus enter the aquatic food web via the diet)[12,42] and be transported downstream during seasonal reservoir destratification.[12–14] Mechanistic information on coupled biogeochemical and hydrologic processes governing Hg(II) and MeHg fate in river-reservoir systems provide opportunities to support strategic management and remediation of Hg in reservoirs.

This study documents a multiyear sampling effort of water and particulate materials of an arid-land reservoir system on the Snake River (the Hells Canyon Complex (HCC); Idaho, Oregon, USA),[13,14,16] which involved quantifying Hg(II) and MeHg dynamics at inflow and outflow locations of three successive hydroelectric reservoirs and with depth in the reservoirs.[43] The goals of the study were to establish linkages between (1) the riverine transport of Hg(II) and MeHg to the reservoirs, (2) seasonal reservoir effects on MeHg formation and partitioning and the role of organic matter composition (DOM, POM), and (3) downstream export of MeHg in water and on particles during reservoir destratification. Seasonal and longitudinal shifts in particulate composition in the first reservoir in the system, Brownlee Reservoir, were quantified using settling traps. The observed spatial and temporal trends in MeHg accumulation in water and on particles in the reservoir, coincident with increases in the organic matter content of particles and MeHg outflow concentrations, provide mechanistic insights on MeHg cycling and fate within and downstream of the reservoir complex. This work builds on companion studies that focused strictly on the magnitude and timing of hydrologic loads of Hg(II) and MeHg into and out of the reservoirs system,[13,14] and parallel efforts of long-term trends in nutrient loading and reservoir anoxia.[29] The implications of these findings are discussed within the context of MeHg bioavailability to aquatic food webs and the dynamics of Hg in managed river-reservoir systems.

Materials and Methods

Site Description

The study was conducted in the HCC, a series of 3 successive hydroelectric reservoirs that span nearly 100 river miles of the Snake River (Idaho, Oregon, USA) (**Figure 1**).[13,44] A complete description of the study basin and properties of the reservoirs are provided in Baldwin et al. (2020)[13] and Naymik et al. (2023).[29] Briefly, the Snake River watershed represents a heavily managed, arid landscape with reservoirs that support flood control, irrigation of neighboring agricultural lands, and hydroelectric power. Brownlee Reservoir, the first reservoir in the HCC, accounts for approximately 86.2% of the total volume capacity of the reservoir complex (with 3.5%, and 10.3% of volume in Oxbow and Hells Canyon reservoirs, respectively), is the deepest (maximum depth of 91 m) and is subject to seasonal drawdown, and has distinct riverine, transition, and lacustrine zones.[29,30] Precise boundaries of the riverine and transition zones vary based on streamflow and reservoir water surface elevation; generally, the riverine zone is between the formal inflow location of Brownlee Reservoir (Snake River mile 345.6) and river mile 325 and the transition zone is between river miles 325 and 308. The boundaries of the lacustrine zone are more consistent and are at river miles 308 and 285 (i.e., Brownlee Dam). The centerline elevation of the penstocks of Brownlee Reservoir is 593.8 m, which governs the vertical location of thermal stratification.[29] Brownlee Reservoir, and to a lesser extent Hells Canyon Reservoir, thermally stratify seasonally and develop hypoxic and anoxic conditions in the metalimnion and hypolimnion.[14,45] For the years of the study, date ranges of high flow versus base flow and the onset and conclusion of reservoir destratification are provided in **Table S1** in the Electronic Supplemental Information (ESI); high flow periods were typically from January-July and destratification periods were typically from July-December.

Water Sample Collection and Processing

Water samples were collected from four locations at inflows and outflows of the reservoir complex including Brownlee Reservoir Inflow (Snake River mile 345.6), Brownlee Reservoir Outflow (Snake River mile 283.9), Oxbow Reservoir Outflow (Snake River mile 269.9), and Hells Canyon Reservoir Outflow (Snake River mile 246.9) (**Figure 1**). Sampling occurred at 2-week intervals during the study (2014-2020). Complete details on the sampling methods at each location are provided in the accompanying data release[43] and companion study.[13] Reservoir outflow locations were downstream of dam tailwaters and therefore were well mixed. Samples were transported on wet ice to Boise, Idaho, for processing within 24 h of collection. The following samples were collected following vacuum filtration through a quartz fiber filter (0.7 µm QFF, pre-combusted at 550° C; Whatman 1851-047): dissolved organic carbon (DOC) concentration and DOM composition measurements (pre-cleaned amber glass bottles, no preservation, stored at 4° C), and total Hg (THg) and MeHg concentrations (pre-cleaned Teflon bottles, 1% v/v 6 M ultra-clean hydrochloric acid). The QFFs were frozen and stored at −20° C for collection of total suspended solids (TSS), particulate THg (p.THg), and particulate MeHg (p.MeHg) samples. Particulate material collected on QFF filters was primarily small organic and inorganic particles, the former including phytoplankton. Mean daily streamflow at Brownlee Inflow were obtained from USGS stream gage station 13269000.[46] The study period spanned a range of Snake River hydrologic conditions including historically high flow conditions (2017), moderate-high flow conditions (2018-2019), and historically low flow conditions (2014-2016, 2020) (**ESI Figure S1**).

In 2017 and 2018, water samples were also collected at 4 locations within Brownlee Reservoir that span the transition and lacustrine zones of the reservoir.[29] Depth profiles were collected between March and December of each year to target seasonal in-reservoir processes from the spring high flows to summer stratified conditions and through the conclusions of reservoir destratification.[14] In-reservoir samples were collected from the water surface (2 meters depth) to above the sediment-water interface

using a peristaltic pump and Teflon tubing (100 meters length, pre-cleaned with 1% hydrochloric acid). The depths of sampling in lacustrine sites of the reservoir (river miles 300 and 286) targeted epilimnetic, metalimnetic, and hypolimnetic strata, as determined by measured temperature profiles[43] and the relative thermal resistance to mixing (comparable to the analysis in Naymik et al. (2023)).[29] The Teflon tubing was rinsed with 30 L of site water at each depth before sample collection, which included an unfiltered sample (collected in a 2 L polyethylene terephthalate (PETE) bottle for processing of Hg samples and TSS) and filtered samples (0.45 µm GeoTech Versapor capsule filter) for DOC concentration and DOM composition measurements (collected in pre-cleaned amber glass bottles, no preservation, stored at 4° C). QFF filtration was conducted within 24 h of sample collection for filter-passing (f.THg and f.MeHg) and particulate measurements (p.THg, p.MeHg, and TSS) of in-reservoir samples. Field replicates were collected and accounted for 10% of total samples. Multiparameter Sonde profiles were collected concurrent to water sampling and are available in the associated data release[43] including dissolved oxygen concentration, oxidation-reduction potential, pH, specific conductance, and turbidity.

Water and Particle Analyses

DOC concentration was determined by persulfate oxidation. UV-vis absorption spectra were measured from 190-800 nm and decadic absorbance values were converted to absorption coefficients as

$$\alpha_\lambda = \frac{A_\lambda}{l} \quad (1)$$

where α_λ is the decadic absorption coefficient (cm^{-1}), A_λ is the absorbance, and l is the path length (cm).[47] The DOM specific ultraviolet absorbance at 254 nm ($SUVA_{254}$), a proxy for DOM aromaticity[47] that indicates DOM source and reactivity to Hg(II),[11,15,39] was calculated by dividing the α_{254} (m^{-1}) by DOC

concentration (mg L^{-1}). Spectral slopes were determined at wavelengths 275 to 295 nm($S_{275\text{-}295}$) and 350 to 400 nm ($S_{350\text{-}400}$).[48] The spectral slope ratio (S_R) was calculated as the $S_{275\text{-}295}$ divided by $S_{350\text{-}400}$.

Mercury measurements were made at the U.S. Geological Survey Mercury Research Laboratory (Madison, WI) (complete details in the associated data release).[43] THg was quantified by cold vapor atomic fluorescence spectroscopy (CVAFS) following EPA method 1631 on a Tekran 2500 (average daily detection limit (DDL) of 42 pg L^{-1}). MeHg was analyzed by isotope dilution, isothermic gas chromatography separation (MERX, Brooks-Rand), and detection by inductively-coupled plasma-mass spectrometry (Thermo Scientific, iCAP ICP-MS) (average DDL of 6 pg L^{-1}). Concentration of filter-passing and volumetric particulate Hg(II) (f.Hg(II) and p.Hg(II), respectively) were calculated as:

$$\text{f.Hg(II)} = \text{f.THg} - \text{f.MeHg} \quad (2)$$

$$\text{p.Hg(II)} = \text{p.THg} - \text{p.MeHg} \quad (3)$$

Dissolved gaseous Hg, reported at <0.2 ng L^{-1} in freshwaters,[49,50] was assumed to have minimal influence on calculated f.Hg(II) values. Gravimetric concentrations of Hg(II) and MeHg, a metric on a particle mass basis (ng g^{-1}), were calculated by dividing volumetric p.Hg(II) and p.MeHg concentration by the TSS concentration, respectively. Distribution coefficients of Hg(II) and MeHg (K_d Hg(II) and K_d MeHg, respectively) were determined as

$$K_\text{d}\ \text{Hg(II)} = \frac{\text{grav. p.Hg(II)}}{\text{f.Hg(II)}} \quad (4)$$

$$K_\text{d}\ \text{MeHg} = \frac{\text{grav. p.MeHg}}{\text{f.MeHg}} \quad (5)$$

where gravimetric p.Hg(II) and p.MeHg concentrations are in units of ng kg^{-1}. K_d values for Hg(II) and MeHg were omitted if filter-passing and particulate concentrations were censored due to measured values being below daily detection limits (*n*=35 of 643 total measurements and *n*=24 of 677 total measurements, respectively).[43] Statistical comparisons between discrete variables were assessed using

linear regression analysis and paired t-tests (SigmaPlot v.14.5) and p-values < 0.05 were considered of statistical significance.

Settling Trap Deployment and Analyses

Particulate material settling in Brownlee Reservoir was collected in cylindrical settling traps (0.015 m^2 opening, Saarso, Hydro-Bios Apparatebau GmbH) deployed at a maximum of three depths at three locations (Snake River miles 318, 300, and 286), which span the transition and lacustrine zones of the reservoir. A total of 16 deployments at all sites and depths were carried out between March 2017 and September 2018; each deployment spanned a maximum of 14 days to minimize the microbial alteration of materials within collection vessels before retrieval. Each deployment depth targeted discrete epilimnetic, metalimnetic, and hypolimnetic strata of Brownlee Reservoir based on temperature profiles.[29] Replicate deployments at identical depths (*n*=8) assessed reproducibility. Within 24 h of retrieval, the settling trap material was sieved (retaining material <243 μm) and analyzed for THg, MeHg, and organic matter content by loss on ignition.[51] Complete information on all the analyses of settling trap material is provided in the associated data release.[43] The relative standard deviation between settling trap field replicates for MeHg concentration and organic matter content averaged 4.6% and 2.5%, respectively (*n*=8).

Results and Discussion

Dissolved Organic Matter Dynamics at Reservoir Inflow and Outflow Locations

Dissolved organic carbon (DOC) concentration and DOM composition exhibited strong temporal dynamics at reservoir inflow and outflow locations based on seasonality and flow conditions (**Figure 2a**). Within each calendar year, two maxima in DOC concentration were observed at Brownlee Reservoir

Inflow (BL Inflow; **Figure 2b**). First, in winter and early spring (Feb. – March) DOC concentrations increased from approximately 2 mg L^{-1} to as high as 5 mg L^{-1} during periods of high flow and then declined to approximately 2.5-3.0 mg L^{-1} with the receding hydrograph (asterisk in **Figure 2b**). The magnitude of increases in DOC concentration during the spring high flow period qualitatively aligned with the magnitude of spring flow over the study period, with substantial increases observed during high flow years (2017, 2019) and relatively muted responses observed during low flow years (2014-2016, 2020). Second, during August baseflow conditions each year, DOC concentrations increased from 3.0 mg L^{-1} to maxima of ~4 mg L^{-1} (arrows in **Figure 2b**). The second maxima in DOC concentration were observed each year regardless of the spring flow condition. Following the second maxima, DOC concentrations decreased to minima of < 2.0 mg L^{-1} from December to February.

The composition of DOM that entered Brownlee Reservoir, as indicated by UV-vis optical metrics including the DOM $SUVA_{254}$ (**Figure 2c**)[47] and spectral slope ($S_{275\text{-}295}$) (**Figure 2d**),[48] provide insight into the source(s) of DOM to the reservoir complex across the hydrograph. Coincident with elevated DOC concentrations during spring high flow were marked increases in the DOM $SUVA_{254}$ (from <2.0 to as high as 3.7 L mgC^{-1} m^{-1}), indicating that DOM entering the reservoir complex during spring high flow is more aromatic,[47,48] of terrestrial origin,[31,52] and of higher reactivity as it pertains to mercury bioavailability.[35,36,38] Consistent with the abovementioned observations of DOC concentration, the magnitude of increases in DOM $SUVA_{254}$ during high flow periods are greater during high flow years (2017, 2019) (asterisk in **Figure 2c**), interpreted to reflect DOM mobilization from terrestrial sources (e.g., surficial soils) at the onset of snowmelt.[52] In contrast, DOM composition during the second maxima in DOC concentration in August was of low aromatic quality (DOM $SUVA_{254}$ < 2.0 L mgC^{-1} m^{-1}), which indicates that the DOM entering the reservoir during base flow was primarily of aquatic origin (e.g., algae exudates).[31,32]

The seasonal dynamics of DOC concentration and DOM composition across all three reservoirs were mainly controlled by the inflowing Snake River (**Figure 2**) as opposed to biogeochemical processes within the three reservoirs. During high flow conditions in the spring, there were no discernable shifts in DOC concentration or DOM composition between the four reservoir inflow-outflow locations (BL Inflow, BL Outflow, OX Outflow, HC Outflow), interpreted to reflect the relatively short residence time of water during high flow.[53] Marginal decreases in DOC concentration (≤ 0.5 mg L^{-1}) and increases in DOM spectral slope ($S_{275\text{-}295}$; ≤ 2.0x10^{-3} nm^{-1}) were observed during base flow conditions between the Brownlee Reservoir Inflow and Outflow, with no further differences observed in these parameters downgradient between Brownlee Reservoir Outflow (BL Outflow) and Hells Canyon Reservoir Outflow (HC Outflow). We interpret these modest shifts between Brownlee Reservoir Inflow and Outflow to reflect a combination of microbial DOC mineralization and autochthonous DOM production in Brownlee Reservoir.[31,33,53] Processes considered to be of lower importance include the photochemical alteration of DOM, due to the low surface-area-to-volume ratio of the reservoirs,[13,48,54] and physical removal of DOC due to DOM sorption or flocculation, provided the high pH (>7.5) of Snake River water.[43]

DOC concentrations in the Snake River were low and the DOM composition was primarily aliphatic, conditions consistent with other reaches of the Snake River[55] and arid-land rivers of the Western United States[56] with low wetland cover.[57] The upgradient processes controlling the inflow of DOM to the reservoirs, including seasonal DOM mobilization from surficial soils and autochthonous DOM production, largely governed DOC concentration and DOM composition throughout the HCC. Extensive eutrophication and impoundments of the Snake River and contributing tributaries[29] upgradient of the HCC likely dampens the influences of HCC reservoirs on DOC concentration and DOM composition,[31–33,53] as supported by the autochthonous nature of DOM entering the reservoirs and only minor shifts in DOM composition observed across the reservoir system. These observations provide a foundation to interpret DOM controls on Hg(II) and MeHg behavior across the HCC.

Hg(II) and MeHg Dynamics at Reservoir Inflow and Outflow Locations

During 2017-2020, concentrations and aqueous-particulate partitioning of Hg(II) trended seasonally across the four reservoir inflow and outflow locations (**Figure 3**). The concentration of filter-passing Hg(II) was highest during periods of high flow (**Figure 3a**), when the DOC concentration and DOM $SUVA_{254}$ were highest (**Figure 2b** and **2c**, respectively). During high spring flow, a strong positive correlation is observed between the f.Hg(II) concentration and DOM α_{254} (**Figure 4**, $R^2 = 0.67$, $p<0.001$), the latter being an optical proxy that positively scales with both DOC concentration and DOM $SUVA_{254}$. Independent correlations between f.Hg(II) and DOC concentration or DOM $SUVA_{254}$ were also significant but of lower correlation coefficient (**ESI Figure S2,** $R^2 = 0.58$ and 0.44, respectively; $p<0.001$). Thus, the f.Hg(II) concentrations entering the reservoirs under high flow conditions are interpreted to reflect Hg(II) co-mobilized with terrestrial DOM from surficial soils of the upgradient watershed. Similar observations have been made in other riverine systems larger and smaller than the Snake River,[19–23] a co-mobilization phenomenon explained by the strong binding of Hg(II) to DOM thiol groups.[58] In contrast, under base flow conditions, f.Hg(II) concentrations were lower (0.2-0.5 ng L^{-1}; **Figure 3a**) and coincide with lower DOC concentration and more autochthonous DOM (i.e., low DOM $SUVA_{254}$) (**Figure 2**). Seasonal trends in f.Hg(II) concentrations observed at Brownlee Inflow were also observed at the three reservoir outflow locations. Yet, discernable decreases in f.Hg(II) concentration (of as much as 0.5 ng L^{-1}) were observed between Brownlee Inflow and Brownlee Outflow, particularly during base flow conditions, for reasons described in a subsection below.

Particulate Hg(II) levels, both p.Hg(II) concentrations in water (ng L^{-1}) and on a particle mass basis (ng g^{-1}), exhibited seasonal trends and shifts between Brownlee Reservoir Inflow and the three reservoir outflow locations. First, p.Hg(II) concentrations (ng L^{-1}) (**Figure 3b**) were elevated at Brownlee Reservoir Inflow primarily during high flow when TSS concentration was highest (**ESI Figure S3b**), explained by the

association of Hg(II) to POM mobilized during high flow.[24] A notable decrease in p.Hg(II) concentration in water was observed between Brownlee Reservoir Inflow and Outflow, consistent with previous documentation of Brownlee Reservoir being a net sink for particulate Hg(II) (on average −52.2 g p.Hg(II) d^{-1})[13] and reservoirs, in general, being sinks for particulates, including POM.[28] Second, the mean concentration of Hg(II) on particles (ng g^{-1}) nearly doubled between Brownlee Reservoir Inflow and Outflow (from 40.5 ng g^{-1} to 73.2 ng g^{-1}, respectively). Downstream of Brownlee Reservoir, there were minimal changes in f.Hg(II) or p.Hg(II) concentrations based on outflow data from Oxbow and Hells Canyon reservoirs, indicating that processes that influence aqueous and particulate Hg(II) fate within the HCC primarily occurred in Brownlee Reservoir.

Methylmercury (MeHg) exhibited seasonal and spatial trends in concentration and filtered-particulate distribution (**Figure 5**) that contrast the abovementioned trends of Hg(II). At Brownlee Reservoir Inflow, f.MeHg concentrations were of low correlation to inflowing DOC concentration and DOM composition (R^2 = 0.11 and 0.04, respectively; **ESI Figure S4**), and were highest in summer reaching maxima of ~0.10 ng L^{-1} (**Figure 5a**). Higher inflow MeHg concentration at base flow[21,59] has been attributed to in-stream and riparian MeHg production.[27] Counter, the volumetric p.MeHg concentration (ng L^{-1}) entering the reservoir complex correlated to the inflowing TSS concentration and was elevated during high spring flow (**ESI Figure S3c**). Importantly, the gravimetric MeHg concentration on particles was largely temporally uniform at Brownlee Reservoir Inflow (3.3±5.2 ng g^{-1}; avg±std, *n*=98) (**Figure 5c**). In marked contrast to trends at Brownlee Reservoir Inflow, higher gravimetric p.MeHg concentrations were observed at Brownlee Reservoir Outflow (**Figure 5c**),particularly under base flow conditions when the reservoir was stratified or undergoing destratification (an increase from 3.72±7.11 ng g^{-1} (*n*=49) to 14.7±15.5 ng g^{-1} (*n*=49); *p*<0.001, t-test). Furthermore, elevated gravimetric concentrations of p.MeHg were also observed at Oxbow and Hells Canyon reservoir outflow locations comparable to Brownlee Reservoir Outflow during Brownlee Reservoir destratification (**Figure 5**).

Shifts in filter-passing and particulate Hg(II) and MeHg concentrations between Brownlee Reservoir Inflow and Outflow had pronounced effects on Hg distribution coefficients (K_d) (**Figure 6b** and **6c**), a parameter representing the competition between filtered and particulate ligands for Hg(II) and MeHg. The average log K_d of Hg(II) and MeHg at Brownlee Reservoir Inflow were 4.89 and 4.83 (n=94 and 97, respectively), respectively (ranging from 4.48-5.92 and 4.17-6.35, respectively). The average log K_d of Hg(II) and MeHg at Brownlee Reservoir Outflow were 5.28 and 5.35 (n=95 and 98, respectively), respectively (ranging from 4.30-5.93 and 4.58-6.06, respectively). The increases in log K_d for Hg(II) and MeHg observed between Brownlee Reservoir Inflow and Outflow were greatest under base flow conditions when the reservoir was undergoing destratification, with differences as high as one order of magnitude (**Figure 6**). No notable changes in the log K_d of Hg(II) and MeHg were observed downstream of Brownlee Reservoir, reinforcing that the redistribution of Hg(II) and MeHg between aqueous and particulate phases within the HCC primarily occurred at Brownlee Reservoir.

Observed differences in log K_d values at reservoir inflow and outflow locations could only partially be attributed to water quality conditions. Lower log K_d values of both Hg(II) and MeHg were observed consistently in the presence of more aromatic DOM (higher $SUVA_{254}$), higher DOC concentration, and higher TSS concentration (**ESI Figure S5)**. However, log K_d values were not explained by any single variable as all three parameters (DOC concentration, DOM $SUVA_{254}$, or TSS) co-varied with spring flow at the Brownlee Reservoir inflow. Higher DOC concentration and higher DOM $SUVA_{254}$ likely limit the partitioning of Hg(II)[58] and MeHg to particles (i.e., lower K_d values), which is consistent with observations in other riverine environments.[21] In addition, lower K_d values at higher TSS concentrations may reflect the effect of particle composition on Hg(II) and MeHg particle concentrations. If particles at Brownlee Reservoir Inflow (**ESI Figure S3a**) have lower organic matter content than reservoir outflow locations, and thus are less efficient at binding Hg(II) and MeHg,[60,61] this could help explain differences in K_d values. Notably, K_d values of Hg(II) and MeHg were the same magnitude and exhibited notable scatter under

base flow conditions when the reservoir was stratified or undergoing destratification (**Figure 6**); the latter observation may result from low TSS masses at this time of year used in K_d calculations (Eq. 4, 5). Below we evaluate the biogeochemical and hydrologic processes within Brownlee Reservoir that help explain observed shifts in aqueous-particulate partitioning and Hg concentrations between Brownlee Reservoir Inflow and Outflow locations.

In-Reservoir Processes: Methylmercury Accumulation and Particle Enrichment

Changes in Hg speciation and aqueous-particulate partitioning observed between Brownlee Reservoir Inflow and Outflow were evaluated with depth profile data collected at four locations within the reservoir at high temporal resolution. The four locations spanned the transition zone (sampled at river miles 318 and 310) and the lacustrine zone of Brownlee Reservoir (sampled at river miles 300 and 286). Seven depth profiles were collected between March–November of 2017 and thirteen depth profiles were collected between April–December of 2018, each targeting reservoir strata present at the time of sampling (epilimnion, metalimnion, and hypolimnion). Profiles of ancillary measurements (DOC, $SUVA_{254}$, α_{254}, and TSS), Hg(II) and MeHg concentrations in water and on particles, and K_d values are presented in ESI Figures S6-S13 and animated electronic supplemental information files. Dissolved oxygen concentration and temperature heat maps of Brownlee Reservoir that were collected during in-reservoir sampling are available in companion studies.[14,29]

At river mile 318, which is at the upstream portion of the transition zone where the velocity of the Snake River decreases,[29] concentrations of TSS, DOC, Hg(II), and MeHg largely reflect seasonal fluctuations of upgradient riverine conditions measured at Brownlee Reservoir Inflow (**ESI Figure S6 and S7**). The ranges of measured parameters at river mile 346 are presented as vertical hashed lines in Figures S6 and S7 for comparison with depth profiles at river mile 318. Temporal decreases in TSS, DOC,

and p.Hg(II) concentrations were observed from high spring flow to base flow each year. Concentrations of Hg(II) and MeHg on a particle mass basis (gravimetric p.Hg(II) and p.MeHg, ng g^{-1}) greatly exceeded those observed at Brownlee Reservoir Inflow in 2017 but were within those observed at Brownlee Reservoir Inflow in 2018. The water column at river mile 318 exhibited anoxic conditions only briefly at depth early during the stratification period (May-July) and the extent of anoxia varied based on annual hydrology (i.e., high vs. low flow years).[14,29,43] Only marginal MeHg accumulation was observed at depth at river mile 318, as f.MeHg and volumetric p.MeHg concentrations were uniformly low (avg±std of 0.04±0.03 and 0.09±0.07 ng L^{-1}, respectively; *n*=38) throughout the water column over the period sampled.

Within the downgradient portion of the transition zone (river mile 310) and the lacustrine zone (river miles 300 and 286), depth profiles present strong evidence for both MeHg accumulation at depth in Brownlee Reservoir and subsequent hydrologic mobilization during reservoir destratification. First, at river mile 310 (**ESI Figures S8 and S9**), TSS concentrations were substantially lower than at river mile 318 and the seasonal fluctuations in TSS, DOC, and p.Hg(II) concentrations (ng L^{-1} and ng g^{-1}) were largely invariant with depth in the water column. MeHg concentrations (f.MeHg and p.MeHg, ng L^{-1} and ng g^{-1}) were more dynamic; concentrations were low across the water column in March–May and September–December (avg±std of 0.03±0.02 ng L^{-1} f.MeHg, 0.05±0.02 ng L^{-1} volumetric p.MeHg, and 5.78±6.35 ng g^{-1} gravimetric p.MeHg) but elevated in June–August in the metalimnion and hypolimnion. Concentrations of f.MeHg and volumetric p.MeHg at maximum depth were as high as 2.1 and 1.0 ng L^{-1}, respectively, and gravimetric p.MeHg concentrations exceeded 200 ng g^{-1} on a particle mass basis. The log K_d of MeHg was largely uniform with depth in the water column, yet increased temporally through the stratified period, attributed chiefly to increased gravimetric p.MeHg concentrations. The post-August decreases in f.MeHg and p.MeHg concentrations at river mile 310 coincided temporally with

interflow that eroded and flushed metalimnetic water out of the transition zone of Brownlee Reservoir.[14,29]

At the two deep lacustrine sites in Brownlee Reservoir (river miles 300 and 286), MeHg concentrations (f.MeHg and p.MeHg) progressively increased in the metalimnion and hypolimnion to maxima in late September of each year, exceeding 3.0 and 0.6 ng L^{-1}, respectively (**ESI Figures S10-S13**). Though TSS concentrations were low in the hypolimnion of Brownlee Reservoir, gravimetric p.MeHg concentrations exhibited a monotonic increase with depth in the reservoir, exceeding 500 ng g^{-1} in several sampling events and locations. For comparison, gravimetric p.MeHg concentrations in the hypolimnion at these sites were two orders of magnitude greater than concentrations observed at Brownlee Reservoir inflow (avg = 3.3±5.2 ng g^{-1}). p.Hg(II) concentrations on a particle mass basis were also elevated in the hypolimnion of Brownlee Reservoir, and increased with depth during the stratified and destratification period, and at times exceeded 1000 ng g^{-1}. Concentrations of f.Hg(II) also exhibited elevated concentrations in the hypolimnion compared to epilimnion in both 2017 and 2018. Elevated hypolimnetic f.Hg(II) can, in part, be explained by the stratification of Brownlee Reservoir that trapped water with high f.Hg(II) and DOC from spring high flow (**Figure 2**). Particle enrichment of Hg(II) and conversion of f.Hg(II) to MeHg likely explains decreases in f.Hg(II) concentration observed between Brownlee Reservoir Inflow and Outflow, whereas other sinks (e.g., photo reduction of Hg(II)) are considered less important due to the low surface-area-to-volume ratio of the reservoir.[13] Elevated gravimetric p.Hg(II) and p.MeHg concentrations were responsible for higher log K_d values of both Hg(II) and MeHg at depth in Brownlee Reservoir. In November 2017 and December 2018, the f.MeHg and volumetric p.MeHg concentrations in the water column were uniformly low at river miles 300 and 286 (avg±std of 0.04±0.04 and 0.03±0.02 ng L^{-1}, respectively; n=12; **ESI Figures S10-S13**), which coincided with the complete destratification of Brownlee Reservoir.[14,29]

A snapshot of the spatial trends in MeHg concentrations and dissolved oxygen observed longitudinally and vertically in Brownlee Reservoir is presented in **Figure 7** (September 2017). Depth profiles of f.MeHg and volumetric p.MeHg concentration (ng L^{-1}; **Figure 7a**) show a systematic increase from upgradient to downgradient in the reservoir and elevated concentrations are observed in the anoxic hypolimnion at river miles 300 and 286. In addition, at river mile 286 elevated concentrations of both f.MeHg and p.MeHg are observed in the metalimnion at the penstock elevation of Brownlee Dam. Gravimetric concentrations of p.MeHg (ng g^{-1}, **Figure 7b**) progressively increased from river mile 318 to 286 across the water column (from 4.50 to 153 ng g^{-1}, respectively). Although this study did not quantify rates of MeHg formation in the water column, though confirmed to be appreciable in an independent study of Brownlee Reservoir during the study period,[11] accumulated MeHg in the hypolimnion is interpreted to result from local internal MeHg production likely associated with the decomposition of settling particles.[62] Elevated MeHg in the metalimnion at river miles 300 and 286 coincided temporally with decreases in MeHg concentrations upgradient in the reservoir and the timing of interflow events within the transition zone.[14,29,45] Thus, metalimnetic MeHg observed at river mile 286 primarily reflects both proximal MeHg production and MeHg hydrologically mobilized from upgradient in the reservoir. The observed seasonal production and mobilization of MeHg in the water column are consistent with observations in other reservoirs.[15,40,42] Although the relative contribution of these two MeHg sources is unknown, we conclude that elevated MeHg in the epilimnion, metalimnion, and hypolimnion in the lacustrine zone of Brownlee Reservoir in late summer and fall is chiefly from internal MeHg production.

We further evaluated temporal trends in particulate Hg concentrations to compare Hg levels within Brownlee Reservoir to those at Brownlee Reservoir Inflow and Outflow locations. Volume-weighted average concentrations of p.MeHg and p.Hg(II) were calculated at three sites within Brownlee Reservoir for the combined epilimnion and metalimnion from discrete depth profiles (see **ESI Section S1** for calculation details; **Table S2**) and compared with p.MeHg and p.Hg(II) concentrations at Brownlee

Reservoir Inflow and Outflow (**Figure 8, ESI Figure S14**). This analysis focused on MeHg on particles in the epilimnion and metalimnion because these strata are relevant to MeHg assimilation in phytoplankton and flow downstream via the penstocks,[14,45] and thus impact downstream food webs.[12] First, gravimetric p.MeHg concentrations at Brownlee Reservoir Inflow were uniformly low across 2017 and 2018 (avg±std of 2.9±3.5 ng g^{-1}; *n*=47) (**Figure 8a**). In stark contrast, during periods of Brownlee Reservoir destratification, subtle increases in gravimetric p.MeHg concentration were observed at river mile 318 and dramatic increases were observed at river miles 300 and 286 (up to 100 ng g^{-1}). Further, systematic temporal increases in gravimetric p.MeHg concentration were observed from upgradient to downgradient (river mile 318 > 300 > 286) during the destratification period of both 2017 and 2018. Increases in gravimetric p.MeHg concentration of similar magnitude were observed at Brownlee Reservoir Outflow shortly after the observed maxima in gravimetric p.MeHg concentration at river mile 286 (**Figure 8a**); these observations demonstrate the progressive downstream mobilization of MeHg formed at depth within Brownlee Reservoir. On average, a 7-fold increase is observed in the mean gravimetric p.MeHg concentration from Brownlee Reservoir Inflow to Outflow during the destratification periods (from 3.32±4.56 to 23.0±17.8 ng g^{-1}, *n*=27 and 25, respectively; *t*-test, $p<0.001$).

Similarly, the percentage of total mercury as MeHg on particles (% p.MeHg) increased systematically within Brownlee Reservoir during the destratification periods to as high as 42% (**Figure 8b**). An analysis was conducted for p.Hg(II) as well (**ESI Figure S14**) that shows a more modest enrichment of particles in Hg(II) within Brownlee Reservoir that aligns with the observed increases in p.Hg(II) concentration on particles between Brownlee Reservoir Inflow and Outflow (**Figure 3c**). In summary, measurements within Brownlee Reservoir demonstrate the enrichment of particles in MeHg (and to a lesser extent Hg(II)) with increased depth in the reservoir, and the hydrologic mobilization of MeHg (as both f.MeHg and p.MeHg) through the reservoir during the destratification of Brownlee Reservoir. Concurrent increases in gravimetric p.MeHg concentration and %MeHg on particles can only be explained by *de*

novo production of MeHg within Brownlee Reservoir and a combination of MeHg adsorption to organic-rich particles (including senescing cells) and active uptake by phytoplankton.[6,7] Thus, in-reservoir MeHg production, increases in organic matter content of particles, and hydrologic flows within Brownlee Reservoir are responsible for shifts in particulate concentrations and log K_d values in Hg(II) and MeHg observed between Brownlee Reservoir Inflow and Outflow.

The compositional evolution of particulate material in Brownlee Reservoir was evaluated to assess potential influences on particulate Hg(II) and MeHg concentrations in the reservoir. Settling traps collected materials from the epilimnion at river mile 318 and epilimnion, metalimnion, and hypolimnion at river miles 300 and 286 (n=16 deployment events from March-November 2017 and 2018). Although marginal differences in the organic matter content of settling trap material were observed between collection depths of a given deployment (epilimnetic vs. metalimnetic vs. hypolimnetic), the time of deployment and longitudinal location had a greater influence on the organic matter content of settling trap materials. A significant increase in the organic matter content of the settling trap materials (<243 μm) was observed between river mile 318 (avg = 12.2%) and river miles 300 (avg = 16.8%) and 286 (avg = 18.7%) (**Figure 9a**). Further, at river miles 300 and 286, the organic matter content of settling trap materials increased from spring to fall (**Figure S15b**), concurrent with expected increases in primary productivity in the reservoir[29,30] and decreases in inorganic particle loading from the upgradient watershed. Across all settling trap deployments at all reservoir locations, the organic matter content of settling trap materials was strongly correlated (R^2 =0.75, p<0.001) with MeHg concentration (ng g^{-1}) (**Figure 9b**). Further, temporal trends in settling trap material MeHg concentration (**ESI Figure S15a**) were consistent with observed trends in gravimetric p.MeHg concentration collected on filters from reservoir water samples (**Figure 8a**). Taken together, the settling trap material results demonstrate the systematic increase in organic matter content of particles within Brownlee Reservoir concurrent with

internal MeHg production, which are interpreted to contribute to the observed enrichment of particles in MeHg within and exported from the reservoir complex.

Synthesis of Processes Governing Mercury Fate in an Arid River-Reservoir System

This study provides a comprehensive spatial and temporal evaluation of processes governing the fate of both Hg(II) and MeHg in water (filtered and associated with particles) in a three-reservoir system spanning nearly 100 river miles. A synthesis of key processes is detailed below, starting at high flow conditions in spring that precede reservoir stratification to the conclusion of the destratification of Brownlee Reservoir in fall.

First, in the spring, particulate Hg(II), particulate MeHg, and filter-passing Hg(II) entered the reservoir under high flow; volumetric particulate Hg(II) and MeHg concentrations were governed by TSS concentration (**ESI Figure S3**) whereas the filter-passing Hg(II) was governed by the concentration of DOM of terrestrial origin (**Figure 4**). At the upgradient transition zone of Brownlee Reservoir, we posit that inorganic-rich particles, anticipated to be deficient in Hg(II) and MeHg,[24,60,61] preferentially settle out of the water column whereas particles with higher organic matter content are transported downgradient. This selective particle settling would explain the observed modest enrichment of particles in both Hg(II) and MeHg in the upgradient transition zone of Brownlee Reservoir (**ESI Figure S8-S9**). In late spring, the onset of thermal stratification established the concentrations of f.Hg(II) in the hypolimnion of the reservoir (**ESI Figure S11**), with higher f.Hg(II) levels under elevated spring flow when terrestrial DOM and f.Hg(II) are delivered to the reservoir complex. Concurrent with thermal stratification, anoxic conditions developed first in the upgradient portion of Brownlee Reservoir[14,29] resulting in Hg(II) methylation in the metalimnion and hypolimnion (**ESI Figures S6-S7**). MeHg accumulated in these strata, in both filter-passing and particulate fractions, and increased longitudinally both up and downgradient in Brownlee Reservoir with the spread of anoxic conditions.[29] MeHg

accumulation in the water column is tentatively attributed primarily to the methylation of water column f.Hg(II) by methylating organisms on sinking particles as they decompose,[11,62] a phenomenon enhanced by the DOM of aromatic quality[38] that is more prevalent in Brownlee Reservoir during high flow years. The processes described above occur between February through early July in this river-reservoir system, when warm inflowing water enters the epilimnion of the reservoir.[29]

Throughout summer (July–September) three important processes occurred concurrently in Brownlee Reservoir: (1) MeHg continued to accumulate in the metalimnion and hypolimnion of the lacustrine zone, reaching maxima in September (**Figure 7**); (2) the organic matter content of particulate material increased (i) temporally and (ii) longitudinally in Brownlee Reservoir (**Figure 9a**), presumably due to autochthonous organic carbon production;[30] and (3) cooler inflowing water that penetrated the metalimnion starting in ~July-August at the transition zone (river miles ~320 – 305),[14,29,45] transporting MeHg as both f.MeHg and p.MeHg downgradient at the depth of the metalimnion towards the penstocks of the Brownlee Dam. This anoxic, MeHg-rich water mixed with epilimnetic and metalimnetic water due to thermal destratification yielding particles with exceptionally high MeHg concentrations and %MeHg (upwards of 100 ng g^{-1} and 42% MeHg, respectively) within the upper layers of Brownlee Reservoir (**Figure 8**). Interflow events incrementally destratified Brownlee Reservoir throughout the late summer and fall (July – December),[29] evidenced by pulses of MeHg-rich water and MeHg-rich particles exiting Brownlee Reservoir[13,14] and exported downstream. The timing of destratification is expected to be dependent on the gradient of the thermocline and density differences between inflowing Snake River water and epilimnetic, metalimnetic, and hypolimnetic reservoir waters.[29] In summary, (1) the biogeochemistry of Brownlee Reservoir enhanced MeHg production and shifts in particle composition, and (2) the stratification-destratification cycle of the reservoir supported efficient downstream export of MeHg (on particles and in water) through both Oxbow and Hells Canyon reservoirs to the downstream Snake River.

This study demonstrates that reservoir impoundment has a multi-dimensional influence on the processes governing MeHg formation and partitioning, both of which play pivotal roles in MeHg uptake in proximal and downstream aquatic food webs.[16] This can be the case both during the early years of impoundment due to decomposition of flooded organic matter,[8,9] and afterwards in some older reservoirs, as described here. Filter-passing and particulate Hg(II) and MeHg concentrations entering Brownlee Reservoir are similar to other riverine systems in the U.S. that receive Hg from upgradient watersheds as a result of atmospheric deposition,[19,21,22,63] yet particles were highly enriched in MeHg exiting the reservoir concurrent with f.MeHg export. We interpret the particle enrichment of MeHg as MeHg uptake by phytoplankton (passive and active uptake to both dead and alive cells)[6,7] due to autochthonous organic carbon production in the reservoir.[13] Provided that gravimetric p.MeHg concentrations averaged 100 ng g^{-1} in the epilimnion and metalimnion (**Figure 8**) and exceeded 500 ng g^{-1} in the hypolimnion of Brownlee Reservoir during fall destratification (**Figure 7**, **Figures S10-13**), we assert that there is high potential for MeHg uptake in aquatic food webs within and downstream of the reservoir complex. For comparison, gravimetric p.MeHg concentrations within and exported from Brownlee Reservoir were comparable to those of a reservoir impaired by local Hg mining (e.g., 100-300 ng g^{-1} MeHg)[42] and hydroelectric reservoirs in South America (≤104 ng g^{-1})[40] and exceeded those observed in subtropical wetlands recognized as MeHg hotspots.[64] Interestingly, log K_d values of MeHg and Hg(II) were of similar magnitude (**Figure 6**), counter to most other environments where Hg(II) K_d values exceed MeHg K_d values by a half order of magnitude. [21,65,66] We suspect that the highly eutrophic state of the river-reservoir system likely enhanced MeHg assimilation in phytoplankton, and the low DOC concentrations of this system and low aromatic quality of DOM, particularly during periods of MeHg production, are insufficient to outcompete organic-rich particles for MeHg.[21] In summary, the elevated p.MeHg concentrations within and exported from Brownlee Reservoir, driven by coupled biogeochemical processes and hydrologic mobilization, likely explain the high bioavailability of MeHg to

the food web in the system[14,16] and other arid reservoirs that stratify.[17] Accounting for mechanistic processes governing Hg(II) and MeHg behavior under variable hydrologic conditions may result in improved management of reservoirs, particularly in the context of climate stressors[18] and changes in nutrient loading.[29] Remediation strategies to reduce Hg uptake in aquatic food webs of reservoirs, whether focused on upgradient nutrient loading to reservoirs or in-reservoir management (e.g., hypolimnetic aeration,[67] oxidant additions),[68] should consider implications of these actions on coupled biogeochemical and hydrologic processes that will ultimately govern responses in Hg(II) and MeHg fate.

Electronic Supporting Information

Electronic supporting information includes details on the calculation of volume-weighted concentrations, tables defining the flow and stratified conditions of Brownlee Reservoir and volume-weighted constituent concentrations, and figures of flow and constituent concentrations in water and of particles at reservoir inflow/outflow locations and within Brownlee Reservoir. Multimedia files of Figures S6-S13 are provided.

Author Contributions

BAP – Conceptualization, methodology, investigation, data curation, formal analysis, writing – original draft

MTT – Conceptualization, methodology, data curation

JO – Investigation

SEB – Investigation, data curation, writing – review & editing

AKB – Conceptualization, investigation, project administration, visualization, writing – review & editing

AMY – Investigation, writing – review & editing

RH – Investigation, resources, writing – review & editing

JN – Conceptualization, resources, writing – review & editing

NG – Conceptualization, investigation, writing – review & editing

CH – Investigation

CL– Investigation

RM – Conceptualization, funding acquisition, writing – review & editing

GRA – Conceptualization, investigation

DPK – Investigation, funding acquisition, project administration, writing – review & editing.

Acknowledgments

Support was provided by the U.S. Geological Survey (USGS) Environmental Health Mission Area's Toxic Substances Hydrology and Contaminants Biology Programs and the Idaho Power Company. We acknowledge three anonymous reviewers and Jacob Fleck (USGS) for constructive comments on the study; Greg Clark (USGS) for initiating the study; Kimberlee Ott, Abby Stover, Grace McCall, and Dominique Rowell (University of Colorado Boulder) for laboratory and field assistance; and Collin Eagles-Smith and James Willacker for helpful discussions. Any use of trade, firm, or product names is for descriptive purposes only and does not imply endorsement by the U.S. Government.

References

(1) UN Environment, 2019, Global Mercury Assessment 2018, UN Environment Programme Chemicals and Health Branch, Geneva Switzerland.

(2) Eagles-Smith, C. A.; Silbergeld, E. K.; Basu, N.; Bustamante, P.; Diaz-Barriga, F.; Hopkins, W. A.; Kidd, K. A.; Nyland, J. F. Modulators of Mercury Risk to Wildlife and Humans in the Context of Rapid Global Change. *Ambio* **2018**. DOI: 10.1007/s13280-017-1011-x.

(3) Obrist, D.; Kirk, J. L.; Zhang, L.; Sunderland, E. M.; Jiskra, M.; Selin, N. E. A Review of Global Environmental Mercury Processes in Response to Human and Natural Perturbations: Changes of Emissions, Climate, and Land Use. *Ambio* **2018**, *47* (2), 116–140. DOI: 10.1007/s13280-017-1004-9.

(4) Peterson, B. D.; Mcdaniel, E. A.; Schmidt, A. G.; Lepak, R. F.; Janssen, S. E.; Tran, P. Q.; Marick, R. A.; Ogorek, J. M.; Dewild, J. F.; Krabbenhoft, D. P.; Mcmahon, K. D. Mercury Methylation Genes Identified across Diverse Anaerobic Microbial Guilds in a Eutrophic Sulfate-Enriched Lake. *Environ. Sci. Technol.* **2020**, 54 (24), 15840-15851. DOI: 10.1021/acs.est.0c05435.

(5) Gilmour, C. C.; Podar, M.; Bullock, A. L.; Graham, A. M.; Brown, S. D.; Somenahally, A. C.; Johs, A.; Hurt, R. A.; Bailey, K. L.; Elias, D. A. Mercury Methylation by Novel Microorganisms from New Environments. *Environ. Sci. Technol.* **2013**, *47* (20), 11810–11820. DOI: 10.1021/es403075t.

(6) Pickhardt, P. C.; Fisher, N. S. Accumulation of Inorganic and Methylmercury by Freshwater Phytoplankton in Two Contrasting Water Bodies. *Environ. Sci. Technol.* **2007**, *41* (1), 125–131. DOI: 10.1021/es060966w.

(7) Moye, H. A.; Miles, C. J.; Phlips, E. J.; Sargent, B.; Merritt, K. K. Kinetics and Uptake Mechanisms for Monomethylmercury between Freshwater Algae and Water. *Environ. Sci. Technol.* **2002**, *36* (16), 3550–3555. DOI: 10.1021/es011421z.

(8) Bilodeau, F.; Therrien, J.; Schetagne, R. Intensity and Duration of Effects of Impoundment on Mercury Levels in Fishes of Hydroelectric Reservoirs in Northern Québec (Canada). *Inl. Waters* **2017**, *7* (4), 493–503. DOI: 10.1080/20442041.2017.1401702.

(9) Bodaly, R. A. (Drew); Jansen, W. A.; Majewski, A. R.; Fudge, R. J. P.; Strange, N. E.; Derksen, A. J.; Green, D. J. Postimpoundment Time Course of Increased Mercury Concentrations in Fish in Hydroelectric Reservoirs of Northern Manitoba, Canada. *Arch. Environ. Contam. Toxicol.* **2007**, *53* (3), 379–389. DOI: 10.1007/s00244-006-0113-4.

(10) Liu, B.; Yan, H.; Wang, C.; Li, Q.; Guédron, S.; Spangenberg, J. E.; Feng, X.; Dominik, J. Insights into Low Fish Mercury Bioaccumulation in a Mercury-Contaminated Reservoir, Guizhou, China. *Environ. Pollut.* **2012**, *160*, 109–117. DOI: 10.1016/j.envpol.2011.09.023.

(11) Eckley, C. S.; Luxton, T. P.; Knightes, C. D.; Shah, V. Methylmercury Production and Degradation under Light and Dark Conditions in the Water Column of the Hells Canyon Reservoirs, USA. *Environ. Toxicol. Chem.* **2021**, *40* (7), 1829–1839. DOI: 10.1002/etc.5041.

(12) Kasper, D.; Forsberg, B. R.; Amaral, J. H. F.; Leitão, R. P.; Py-Daniel, S. S.; Bastos, W. R.; Malm, O. Reservoir Stratification Affects Methylmercury Levels in River Water, Plankton, and Fish Downstream from Balbina Hydroelectric Dam, Amazonas, Brazil. *Environ. Sci. Technol.* **2014**, *48* (2), 1032–1040. DOI: 10.1021/es4042644.

(13) Baldwin, A. K.; Poulin, B. A.; Naymik, J.; Hoovestol, C.; Clark, G. M.; Krabbenhoft, D. P. Seasonal Dynamics and Interannual Variability in Mercury Concentrations and Loads through a Three-Reservoir Complex. *Environ. Sci. Technol.* **2020**, 54 (15), 9305-9314. DOI: 10.1021/acs.est.9b07103.

(14) Baldwin, A. K.; Eagles-Smith, C. A.; Willacker, J. J.; Poulin, B. A.; Krabbenhoft, D. P.; Naymik, J.; Tate, M. T.; Bates, D.; Gastelecutto, N.; Hoovestol, C.; Larsen, C.; Yoder, A. M.; Chandler, J.; Myers, R. In-Reservoir Physical Processes Modulate Aqueous and Biological Methylmercury Export from a Seasonally Anoxic Reservoir. *Environ. Sci. Technol.* **2022**, *56* (19), 13751–13760. DOI: 10.1021/acs.est.2c03958.

(15) De Bonville, J.; Amyot, M.; del Giorgio, P.; Tremblay, A.; Bilodeau, F.; Ponton, D. E.; Lapierre, J.-F. Mobilization and Transformation of Mercury Across a Dammed Boreal River Are Linked to Carbon Processing and Hydrology. *Water Resour. Res.* **2020**, *56* (10), e2020WR027951. DOI: 10.1029/2020WR027951.

(16) Clark, G. M.; Naymik, J.; Krabbenhoft, D. P.; Eagles-Smith, C. A.; Aiken, G. R.; Marvin-DiPasquale, M. C.; Harris, R. C.; Myers, R. Mercury Cycling in the Hells Canyon Complex of the Snake River,

Idaho and Oregon; Reston, VA, U.S. Geological Survey Fact Sheet 2016-3051, 6 p. DOI: 10.3133/fs20163051.

(17) Willacker, J. J.; Eagles-Smith, C. A.; Lutz, M. A.; Tate, M. T.; Lepak, J. M.; Ackerman, J. T. Reservoirs and Water Management Influence Fish Mercury Concentrations in the Western United States and Canada. *Sci. Total Environ.* **2016**, *568*, 739–748. DOI: 10.1016/j.scitotenv.2016.03.050.

(18) Martin, J. T.; Pederson, G. T.; Woodhouse, C. A.; Cook, E. R.; McCabe, G. J.; Anchukaitis, K. J.; Wise, E. K.; Erger, P. J.; Dolan, L.; McGuire, M.; Gangopadhyay, S.; Chase, K. J.; Littell, J. S.; Gray, S. T.; St. George, S.; Friedman, J. M.; Sauchyn, D. J.; St-Jacques, J.-M.; King, J. Increased Drought Severity Tracks Warming in the United States' Largest River Basin. *Proc. Natl. Acad. Sci.* **2020**, *117* (21), 11328–11336. DOI: 10.1073/pnas.1916208117.

(19) Dittman, J. A.; Shanley, J. B.; Driscoll, C. T.; Aiken, G. R.; Chalmers, A. T.; Towse, J. E. Ultraviolet Absorbance as a Proxy for Total Dissolved Mercury in Streams. *Environ. Pollut.* **2009**, *157* (6), 1953–1956. DOI: 10.1016/j.envpol.2009.01.031

(20) Dittman, J. a.; Shanley, J. B.; Driscoll, C. T.; Aiken, G. R.; Chalmers, A. T.; Towse, J. E.; Selvendiran, P. Mercury Dynamics in Relation to Dissolved Organic Carbon Concentration and Quality during High Flow Events in Three Northeastern U.S. Streams. *Water Resour. Res.* **2010**, *46* (7), W07522. DOI: 10.1029/2009WR008351.

(21) Brigham, M. E.; Wentz, D. A.; Aiken, G. R.; Krabbenhoft, D. P. Mercury Cycling in Stream Ecosystems. 1. Water Column Chemistry and Transport. *Environ. Sci. Technol.* **2009**, *43* (8), 2720–2725. DOI: 10.1021/es802694n.

(22) Stoken, O. M.; Riscassi, A. L.; Scanlon, T. M. Association of Dissolved Mercury with Dissolved Organic Carbon in U.S. Rivers and Streams: The Role of Watershed Soil Organic Carbon. *Water Resour. Res.* **2016**, *52* (4), 3040–3051. DOI: 10.1002/2015WR017849.

(23) Burns, D. A.; Aiken, G. R.; Bradley, P. M.; Journey, C. A.; Schelker, J. Specific Ultra-Violet Absorbance as an Indicator of Mercury Sources in an Adirondack River Basin. *Biogeochemistry* **2013**, *113*, 451–466. DOI: 10.1007/s10533-012-9773-5.

(24) Hurley, J. P.; Cowell, S. E.; Shafer, M. M.; Hughes, P. E. Partitioning and Transport of Total and Methyl Mercury in the Lower Fox River, Wisconsin. *Environ. Sci. Technol.* **1998**, *32* (10), 1424–1432. DOI: 10.1021/es970685b.

(25) Bradley, P. M.; Burns, D. A.; Murray, K. R.-; Brigham, M. E.; Button, D. T.; Chasar, L. C.; Marvin-DiPasquale, M.; Lowery, M. A.; Journey, C. A. Spatial and Seasonal Variability of Dissolved Methylmercury in Two Stream Basins in the Eastern United States. *Environ. Sci. Technol.* **2011**, *45* (6), 2048–2055. DOI: 10.1021/es103923j.

(26) Poulin, B. A.; Aiken, G. R.; Nagy, K. L.; Manceau, A.; Krabbenhoft, D. P.; Ryan, J. N. Mercury Transformation and Release Differs with Depth and Time in a Contaminated Riparian Soil during Simulated Flooding. *Geochim. Cosmochim. Acta* **2016**, *176*, 118–138. DOI: 10.1016/j.gca.2015.12.024.

(27) Bradley, P. M.; Journey, C. a; Lowery, M. a; Brigham, M. E.; Burns, D. a; Button, D. T.; Chapelle, F. H.; Lutz, M. a; Marvin-Dipasquale, M. C.; Riva-Murray, K. Shallow Groundwater Mercury Supply in a Coastal Plain Stream. *Environ. Sci. Technol.* **2012**, *46* (14), 7503–7511. DOI: 10.1021/es301540g.

(28) Mendonça, R.; Müller, R. A.; Clow, D.; Verpoorter, C.; Raymond, P.; Tranvik, L. J.; Sobek, S.

Organic Carbon Burial in Global Lakes and Reservoirs. *Nat. Commun.* **2017**, *8* (1), 1694. DOI: 10.1038/s41467-017-01789-6.

(29) Naymik, J.; Larsen, C.; Myers, R.; Hoovestol, C.; Gastelecutto, N.; Bates, D. Long-Term Trends in Inflowing Chlorophyll A and Nutrients and Their Relation to Dissolved Oxygen in a Large Western Reservoir. *Lake Reserv. Manag.* **2023**, *39* (1), 53–71. DOI: 10.1080/10402381.2022.2160395.

(30) Kimmel, B. L.; Groeger, A. W. Factors Controlling Primary Production in Lakes and Reservoirs: A Perspective. *Lake Reserv. Manag.* **1984**, *1* (1), 277–281. DOI: 10.1080/07438148409354524.

(31) Kraus, T. E. C.; Bergamaschi, B. A.; Hernes, P. J.; Doctor, D.; Kendall, C.; Downing, B. D.; Losee, R. F. How Reservoirs Alter Drinking Water Quality: Organic Matter Sources, Sinks, and Transformations. *Lake Reserv. Manag.* **2011**, *27* (3), 205–219. DOI: 10.1080/07438141.2011.597283.

(32) Oliver, A. A.; Spencer, R. G. M.; Deas, M. L.; Dahlgren, R. A. Impact of Seasonality and Anthropogenic Impoundments on Dissolved Organic Matter Dynamics in the Klamath River (Oregon/California, USA). *J. Geophys. Res. Biogeosciences* **2016**, *121* (7), 1946–1958. DOI: 10.1002/2016JG003497.

(33) Mash, H.; Westerhoff, P. K.; Baker, L. A.; Nieman, R. A.; Nguyen, M.-L. Dissolved Organic Matter in Arizona Reservoirs: Assessment of Carbonaceous Sources. *Org. Geochem.* **2004**, *35* (7), 831–843. DOI: 10.1016/j.orggeochem.2004.03.002.

(34) Poulin, B. A.; Gerbig, C. A.; Kim, C. S.; Stegemeier, J. P.; Ryan, J. N.; Aiken, G. R. Effects of Sulfide Concentration and Dissolved Organic Matter Characteristics on the Structure of Nanocolloidal Metacinnabar. *Environ. Sci. Technol.* **2017**, *51* (22), 13133–13142. DOI: 10.1021/acs.est.7b02687.

(35) Ravichandran, M.; Aiken, G. R.; Ryan, J. N.; Reddy, M. M. Inhibition of Precipitation and Aggregation of Metacinnabar (Mercuric Sulfide) by Dissolved Organic Matter Isolated from the Florida Everglades. *Environ. Sci. Technol.* **1999**, *33* (9), 1418–1423. DOI: 10.1021/es9811187.

(36) Waples, J. S.; Nagy, K. L.; Aiken, G. R.; Ryan, J. N. Dissolution of Cinnabar (HgS) in the Presence of Natural Organic Matter. *Geochim. Cosmochim. Acta* **2005**, *69* (6), 1575–1588. DOI: 10.1016/j.gca.2004.09.029.

(37) Gerbig, C. A.; Kim, C. S.; Stegemeier, J. P.; Ryan, J. N.; Aiken, G. R. Formation of Nanocolloidal Metacinnabar in Mercury-DOM-Sulfide Systems. *Environ. Sci. Technol.* **2011**, *45* (21), 9180–9187. DOI: 10.1021/es201837h.

(38) Graham, A. M.; Aiken, G. R.; Gilmour, C. C. Effect of Dissolved Organic Matter Source and Character on Microbial Hg Methylation in Hg-S-DOM Solutions. *Environ. Sci. Technol.* **2013**, *47* (11), 5746–5754. DOI: 10.1021/es400414a.

(39) Pestana, I. A.; Azevedo, L. S.; Bastos, W. R.; Magalhães de Souza, C. M. The Impact of Hydroelectric Dams on Mercury Dynamics in South America: A Review. *Chemosphere* **2019**, *219*, 546–556. DOI: 10.1016/j.chemosphere.2018.12.035.

(40) Pestana, I. A.; Bastos, W. R.; Almeida, M. G.; Mussy, M. H.; Souza, C. M. M. Methylmercury in Environmental Compartments of a Hydroelectric Reservoir in the Western Amazon, Brazil. *Chemosphere* **2019**, *215*, 758–765. DOI: 10.1016/j.chemosphere.2018.10.106.

(41) Jones, D. S.; Walker, G. M.; Johnson, N. W.; Mitchell, C. P. J.; Coleman Wasik, J. K.; Bailey, J. V.

Molecular Evidence for Novel Mercury Methylating Microorganisms in Sulfate-Impacted Lakes. *ISME J.* **2019**, 13, 1659-1675. DOI: 10.1038/s41396-019-0376-1.

(42) Seelos, M.; Beutel, M.; McCord, S.; Kim, S.; Vigil, K. Plankton Population Dynamics and Methylmercury Bioaccumulation in the Pelagic Food Web of Mine-Impacted Surface Water Reservoirs. *Hydrobiologia* **2022**, 849 (21), 4803-4822. DOI: 10.1007/s10750-022-05018-0.

(43) Poulin, B. A.; Breitmeyer, S.E. Krabbenhoft, D. P.; Tate, M. T.; DeWild, J. F.; Ogorek, J. M.; Babiarz, C. L.; Janssen, S. E.; Marvin-DiPasquale, M. C.; Agee, J. L.; Kakouros, E.; Kieu, L.; Arias, M.; Conaway, C.; Antweiler, R. C.; Baldwin, A. K.; Yoder, A.; Clark, G. M.; Aiken, G. R. Chemical Characterization of Water and Suspended Sediment of the Snake River and Hells Canyon Complex (Idaho, Oregon). *U.S. Geol. Surv. data release* **2022**, *ver. 2.0*, DOI: 10.5066/P9DT2B6J.

(44) Myers, R.; Harrison, J.; Parkinson, S. K.; Hoelscher, B.; Naymik, J.; Parkinson, S. E. Pollutant Transport and Processing in the Hells Canyon Complex. Technical Report Appendix E.2.2-2. *Idaho Power Co.* **2003**.

(45) Botelho, D. A.; Imberger, J. Dissolved Oxygen Response to Wind-Inflow Interactions in a Stratified Reservoir. *Limnol. Oceanogr.* **2007**, *52* (5), 2027–2052. DOI: 10.4319/lo.2007.52.5.2027.

(46) U.S. Geological Survey. **2021**, USGS Water Data for the Nation: U.S. Geological Survey National Water Information System Database. Accessed January, 1, 2021. DOI: 10.5066/F7P55KJN.

(47) Weishaar, J. L.; Aiken, G. R.; Bergamaschi, B. a; Fram, M. S.; Fujii, R.; Mopper, K. Evaluation of Specific Ultraviolet Absorbance as an Indicator of the Chemical Composition and Reactivity of Dissolved Organic Carbon. *Environ. Sci. Technol.* **2003**, *37* (20), 4702–4708. DOI: 10.1021/es030360x.

(47) Helms, J. R.; Stubbins, A.; Ritchie, J. D.; Minor, E. C.; Kieber, D. J.; Mopper, K. Absorption Spectral Slopes and Slope Ratios as Indicators of Molecular Weight, Source, and Photobleaching of Chromophoric Dissolved Organic Matter. *Limnol. Oceanogr.* **2008**, *53* (3), 955–969. DOI: 10.4319/lo.2008.53.3.0955.

(48) Poulin, B. A.; Ryan, J. N.; Tate, M. T.; Krabbenhoft, D. P.; Hines, M. E.; Barkay, T.; Schaefer, J.; Aiken, G. R. Geochemical Factors Controlling Dissolved Elemental Mercury and Methylmercury Formation in Alaskan Wetlands of Varying Trophic Status. *Environ. Sci. Technol.* **2019**, *53* (11), 6203–6213. DOI: 10.1021/acs.est.8b06041.

(50) Poulain, A. J.; Amyot, M.; Findlay, D.; Telor, S.; Barkay, T.; Hintelmann, H. Biological and Photochemical Production of Dissolved Gaseous Mercury in a Boreal Lake. *Limnol. Oceanogr.* **2004**, *49* (6), 2265–2275. DOI: 10.4319/lo.2004.49.6.2265.

(50) Dean, W. E. Determination of Carbonate and Organic Matter in Calcareous Sediments and Sedimentary Rocks by Loss on Ignition: Comparison with Other Methods. *J. Sediment. Petrol.* **1974**, *44*, 242–248.

(51) Ulseth, A. J.; Hall Jr., R. O. Dam Tailwaters Compound the Effects of Reservoirs on the Longitudinal Transport of Organic Carbon in an Arid River. *Biogeosciences* **2015**, *12* (14), 4345–4359. DOI: 10.5194/bg-12-4345-2015.

(53) Hosen, J. D.; Allen, G. H.; Amatulli, G.; Breitmeyer, S.; Cohen, M. J.; Crump, B. C.; Lu, Y.; Payet, J. P.; Poulin, B. A.; Stubbins, A.; Yoon, B.; Raymond, P. A. River Network Travel Time Is Correlated with Dissolved Organic Matter Composition in Rivers of the Contiguous United States. *Hydrol.*

Process. **2021**, *35* (5), e14124. DOI: 10.1002/hyp.14124.

(53) Hansen, A. M.; Kraus, T. E. C.; Pellerin, B. A.; Fleck, J. A.; Downing, B. D.; Bergamaschi, B. A. Optical Properties of Dissolved Organic Matter (DOM): Effects of Biological and Photolytic Degradation. *Limnol. Oceanogr.* **2016**, *61* (3), 1015–1032. DOI: 10.1002/lno.10270.

(54) Thomas, S. A.; Royer, T. V; Snyder, E. B.; Davis, J. C. Organic Carbon Spiraling in an Idaho River. *Aquat. Sci.* **2005**, *67* (4), 424–433. DOI: 10.1007/s00027-005-0790-5.

(55) Spencer, R. G. M.; Butler, K. D.; Aiken, G. R. Dissolved Organic Carbon and Chromophoric Dissolved Organic Matter Properties of Rivers in the USA. *J. Geophys. Res.* **2012**, *117* (G3), G03001. DOI: 10.1029/2011JG001928.

(56) Spencer, R. G. M.; Aiken, G. R.; Dornblaser, M. M.; Butler, K. D.; Holmes, R. M.; Fiske, G.; Mann, P. J.; Stubbins, A. Chromophoric Dissolved Organic Matter Export from U.S. Rivers. *Geophys. Res. Lett.* **2013**, *40* (8), 1575–1579. DOI: 10.1002/grl.50357.

(58) Haitzer, M.; Aiken, G. R.; Ryan, J. N. Binding of Mercury(II) to Dissolved Organic Matter: The Role of the Mercury-to-DOM Concentration Ratio. *Environ. Sci. Technol.* **2002**, *36* (16), 3564–3570. DOI: 10.1021/es025699i.

(58) Bishop, K.; Lee, Y.-H.; Pettersson, C.; Allard, B. Methylmercury Output from the Svartberget Catchment in Northern Sweden during Spring Flood. *Water. Air. Soil Pollut.* **1995**, *80* (1), 445–454. DOI: 10.1007/BF01189694.

(59) Scherbatskoy, T.; Shanley, J. B.; Keeler, G. J. Factors Controlling Mercury Transport in an Upland Forested Catchment. *Water. Air. Soil Pollut.* **1998**, *105* (1), 427–438. DOI: 1023/A:1005053509133.

(60) Millera Ferriz, L.; Ponton, D. E.; Storck, V.; Leclerc, M.; Bilodeau, F.; Walsh, D. A.; Amyot, M. Role of Organic Matter and Microbial Communities in Mercury Retention and Methylation in Sediments near Run-of-River Hydroelectric Dams. *Sci. Total Environ.* **2021**, *774*, 145686. DOI: 10.1016/j.scitotenv.2021.145686.

(61) Gascón Díez, E.; Loizeau, J.-L.; Cosio, C.; Bouchet, S.; Adatte, T.; Amouroux, D.; Bravo, A. G. Role of Settling Particles on Mercury Methylation in the Oxic Water Column of Freshwater Systems. *Environ. Sci. Technol.* **2016**, *50* (21), 11672–11679. DOI: 10.1021/acs.est.6b03260.

(62) Smith, D. B.; Cannon, W. F.; Woodruff, L. G.; Solano, F.; Ellefsen, K. J. *Geochemical and Mineralogical Maps for Soils of the Conterminous United States*; Reston, VA, 2014. DOI: 10.3133/ofr20141082.

(64) Hurley, J. P.; Krabbenhoft, D. P.; Cleckner, L. B.; Olson, M. L.; Aiken, G. R.; Rawlik, P. S. System Controls on the Aqueous Distribution of Mercury in the Northern Florida Everglades. *Biogeochemistry* **1998**, *40* (2/3), 293–310. DOI: 10.1023/A:1005928927272.

(64) Hammerschmidt, C. R.; Fitzgerald, W. F.; Lamborg, C. H.; Balcom, P. H.; Tseng, C. M. Biogeochemical Cycling of Methylmercury in Lakes and Tundra Watersheds of Arctic Alaska. *Environ. Sci. Technol.* **2006**, *40* (4), 1204–1211. DOI: 10.1021/es051322b.

(65) Kim, E.-H.; Mason, R. P.; Porter, E. T.; Soulen, H. L. The Effect of Resuspension on the Fate of Total Mercury and Methyl Mercury in a Shallow Estuarine Ecosystem: A Mesocosm Study. *Mar. Chem.* **2004**, *86* (3), 121–137. DOI: 10.1016/j.marchem.2003.12.004.

(66) Seelos, M.; Beutel, M.; Austin, C. M.; Wilkinson, E.; Leal, C. Effects of Hypolimnetic Oxygenation on Fish Tissue Mercury in Reservoirs near the New Almaden Mining District, California, USA. *Environ. Pollut.* **2021**, *268*, 115759. DOI: 10.1016/j.envpol.2020.115759.

(67) Beutel, M. W.; Duvil, R.; Cubas, F. J.; Grizzard, T. J. Effects of Nitrate Addition on Water Column Methylmercury in Occoquan Reservoir, Virginia, USA. *Water Res.* **2017**, *110*, 288–296. DOI: 10.1016/j.watres.2016.12.022.

Figures

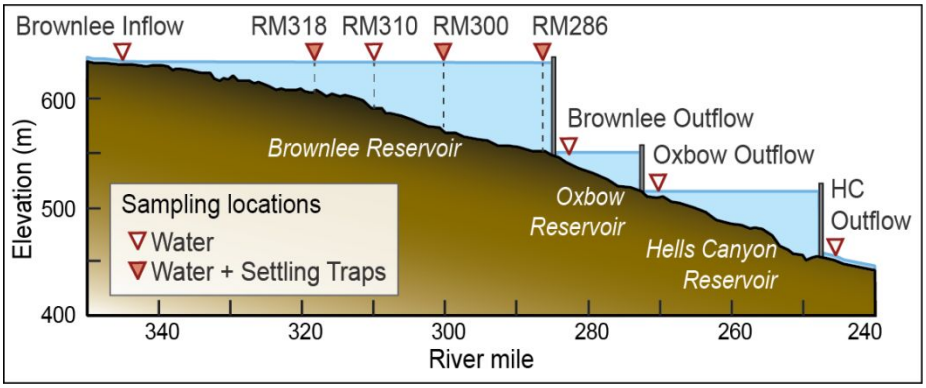

Figure 1. Schematic diagram of the Hells Canyon Complex (HCC, Idaho and Oregon, USA) including locations of reservoir inflow and outflow locations (Brownlee Inflow, RM 345.6; Brownlee Outflow, RM 283.9; Oxbow Outflow, RM 269.9; Hells Canyon (HC) Outflow, RM 246.9) and locations of in-reservoir collection of water and settling trap material (RM 318, 310, 300, and 286) in Brownlee Reservoir.[43] River miles (RM) identify the distance to the confluence of the Snake River and the Columbia River.

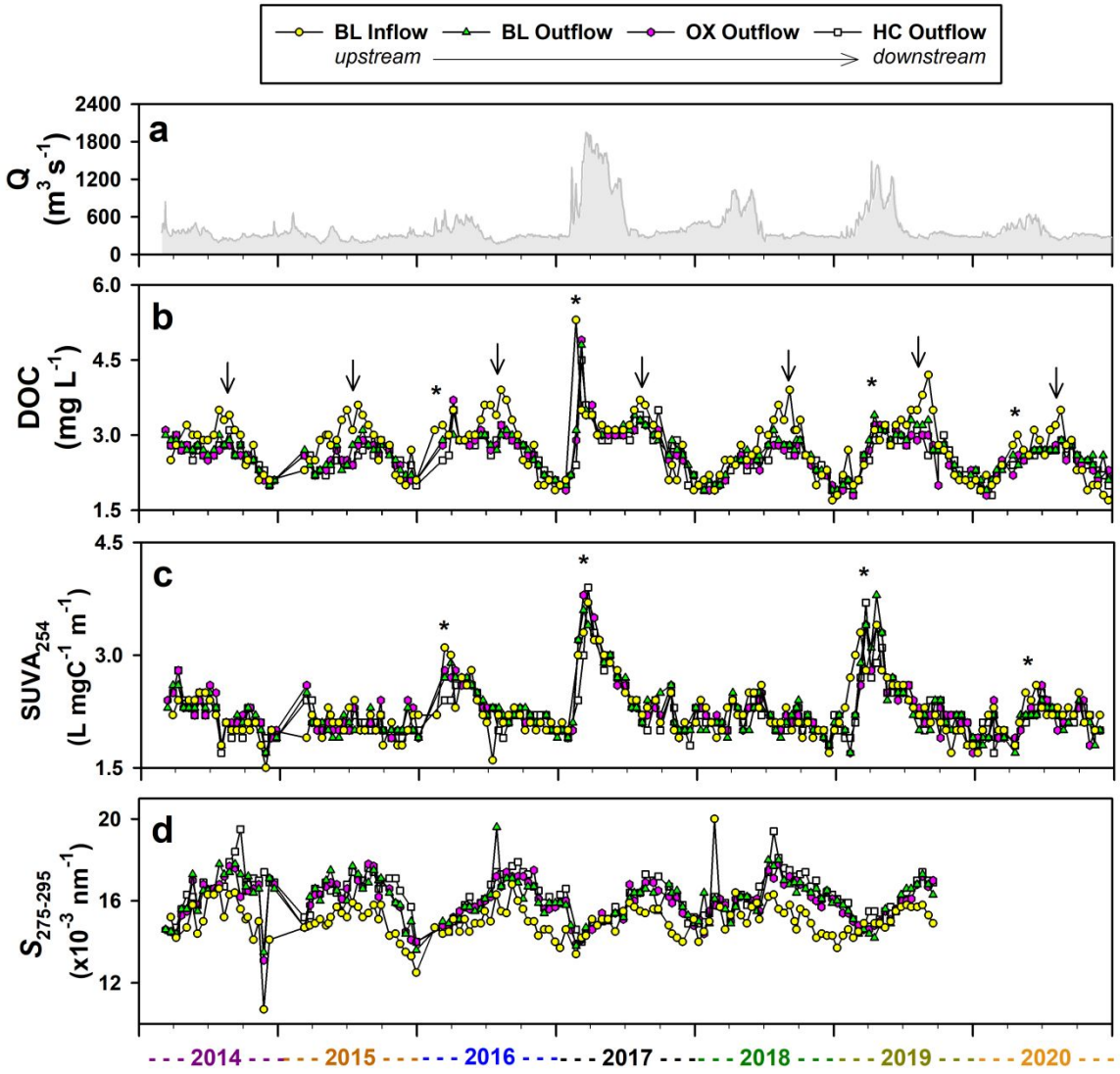

Figure 2. Plots of the (**a**) discharge at Brownlee Reservoir Inflow,[46] (**b**) dissolved organic carbon (DOC) concentration, and dissolved organic matter (**c**) specific ultraviolet absorbance at 254 nm ($SUVA_{254}$) and (**d**) spectral slope from 275-295 nm ($S_{275\text{-}295}$) from 2014 – 2020 at inflow – outflow sites of the Hells Canyon Complex (Brownlee Reservoir Inflow, BL Inflow; Brownlee Reservoir Outflow, BR Outflow; Oxbow Reservoir Outflow, OX Outflow; and Hells Canyon Reservoir Outflow, HC Outflow).[43] Arrows identify DOC maxima observed in August each year, and asterisk symbols identify DOC and $SUVA_{254}$ maxima observed in spring during high-flow years. $S_{275\text{-}295}$ data were not available from October 2019 – 2020.

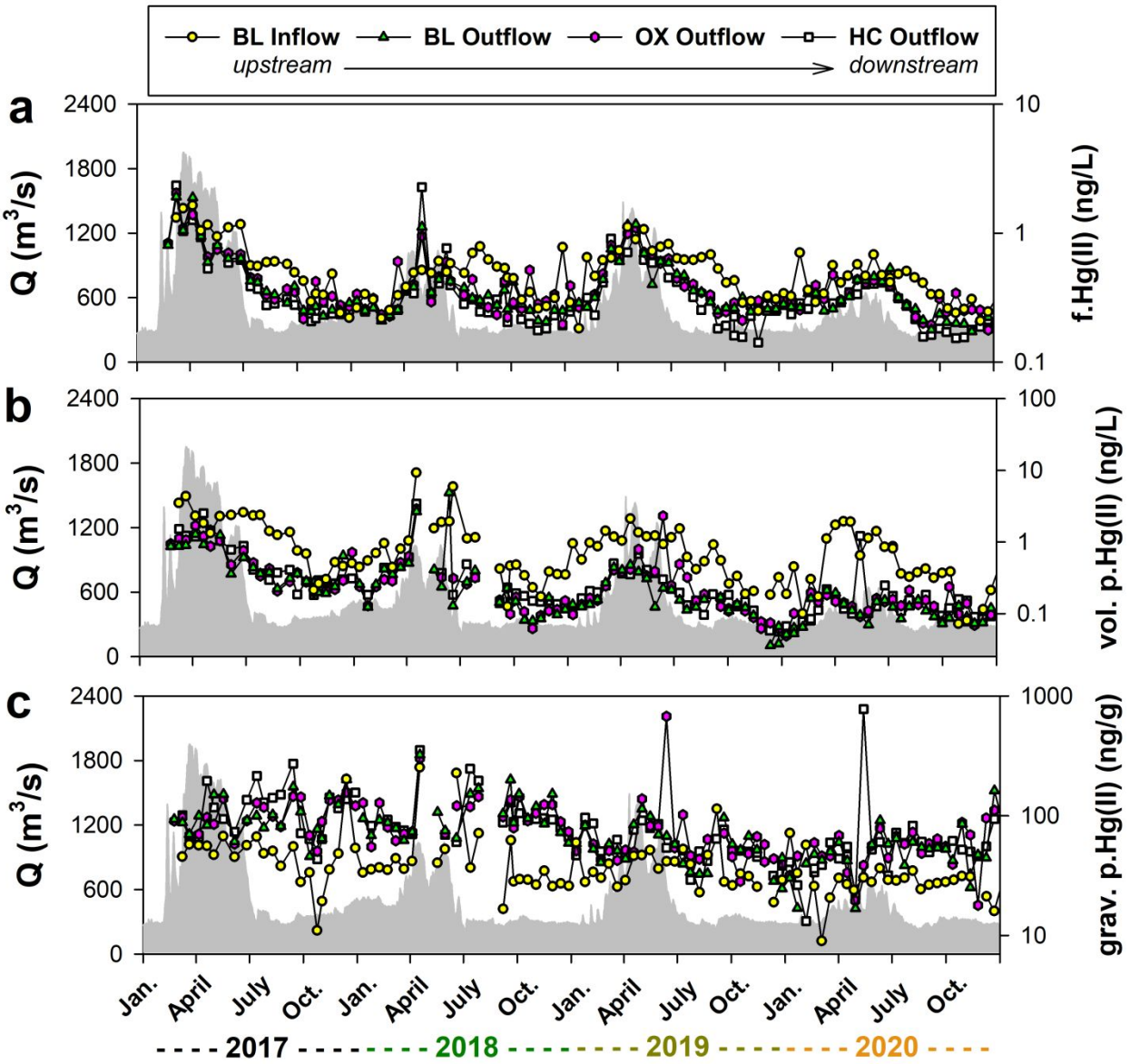

Figure 3. The concentrations of inorganic divalent Hg (Hg(II)) in (**a**) water (filter-passing; f.Hg(II)) and associated with particles, both on a volumetric basis (**b**; vol. p.Hg(II), ng L^{-1}) and a gravimetric basis (**c**; grav. p.Hg(II), ng g^{-1}), from 2017 – 2020 at inflow – outflow sites of the Hells Canyon Complex (Brownlee Reservoir Inflow, BL Inflow; Brownlee Reservoir Outflow, BL Outflow; Oxbow Reservoir Outflow, OX Outflow; and Hells Canyon Reservoir Outflow, HC Outflow).[43] The shaded gray area plot is the discharge at Brownlee Reservoir Inflow.[46]

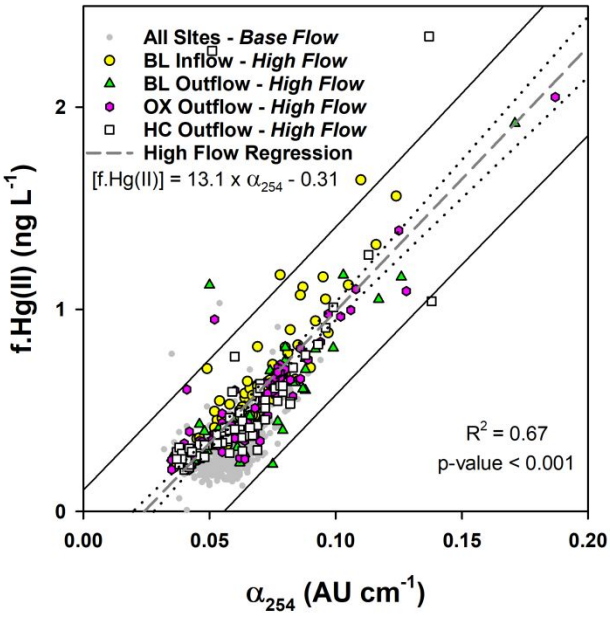

Figure 4. Scatter plot and linear regression line between filter-passing Hg(II) (f.Hg(II)) and the absorbance of the DOM at 254 nm (α_{254}) at inflow and outflow sites of the Hells Canyon Complex.[43] The dashed gray, dotted black, and solid black lines present the linear fit of data, 95% confidence interval of the fit, and prediction interval of the fit, respectively, for samples collected under high flow conditions (*n*=271; see Table S1 in the ESI for definitions).

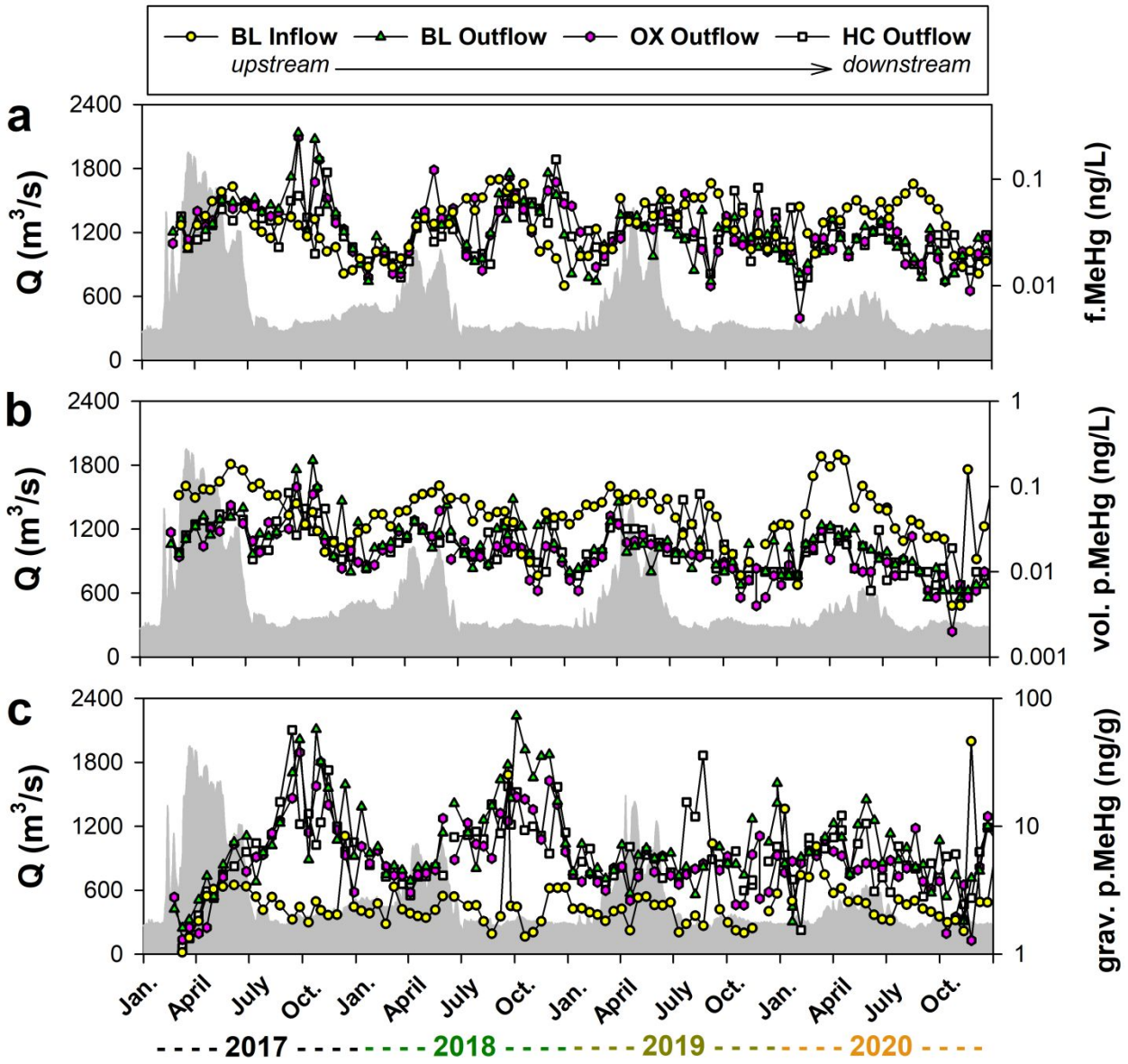

Figure 5. The concentrations of methylmercury (MeHg) in (**a**) water (filter-passing; MeHg) and associated with particles, both on a volumetric basis (**b**; vol. p.MeHg, ng L^{-1}), and on a gravimetric basis (**c**; grav. p.MeHg, ng g^{-1}), from 2016 – 2020 at inflow – outflow sites of the Hells Canyon Complex (Brownlee Reservoir Inflow, BL Inflow; Brownlee Reservoir Outflow, BL Outflow; Oxbow Reservoir Outflow, OX Outflow; and Hells Canyon Reservoir Outflow, HC Outflow).[43] The shaded gray area plot is the discharge at Brownlee Reservoir Inflow.[46]

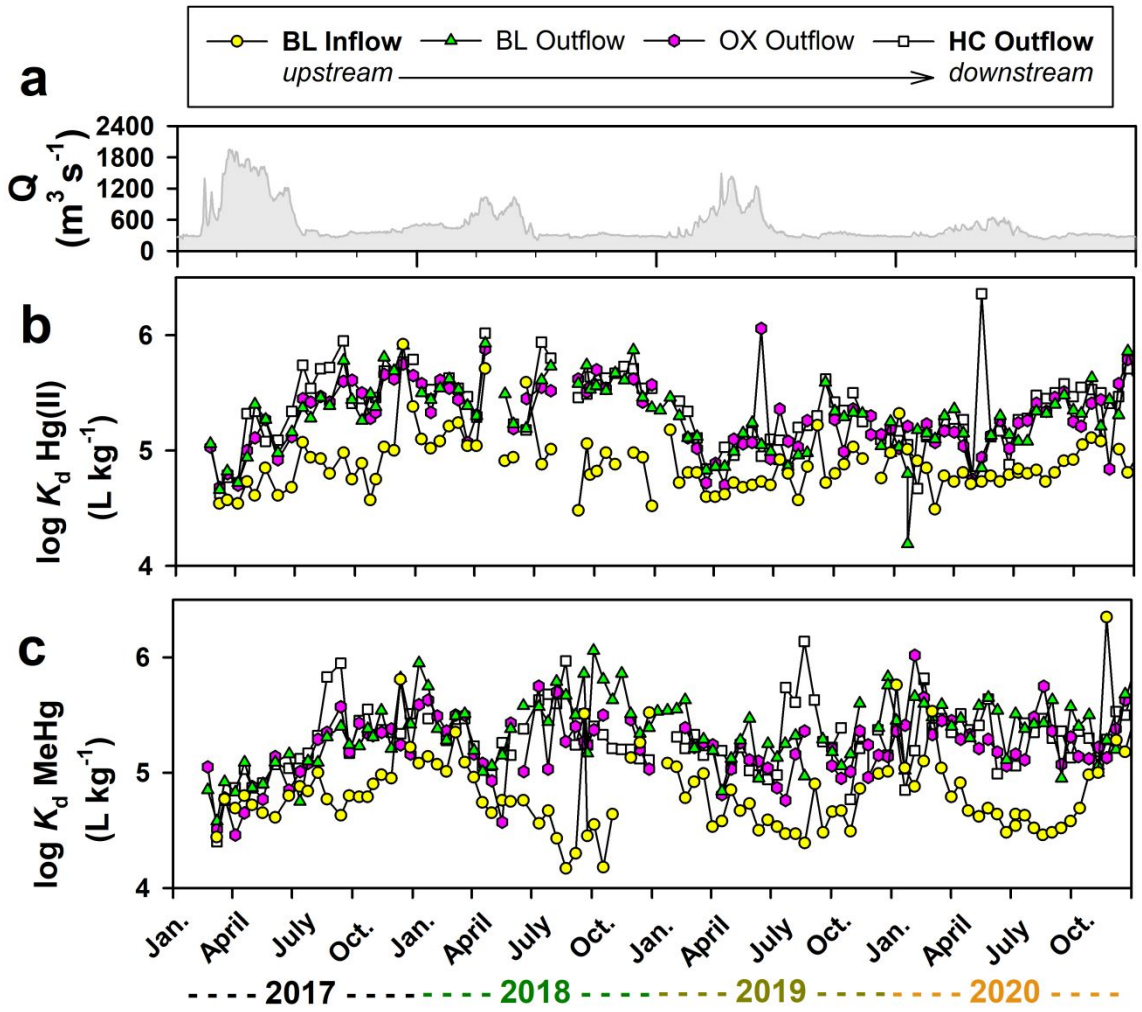

Figure 6. Plots of the (**a**) discharge[46] and (**b**, **c**) log-transformed distribution coefficients (log K_d) of Hg(II) and MeHg from 2017 – 2020 at inflow – outflow sites of the Hells Canyon Complex (Brownlee Reservoir Inflow, BL Inflow; Brownlee Reservoir Outflow, BL Outflow; Oxbow Reservoir Outflow, OX Outflow; and Hells Canyon Reservoir Outflow, HC Outflow).[43]

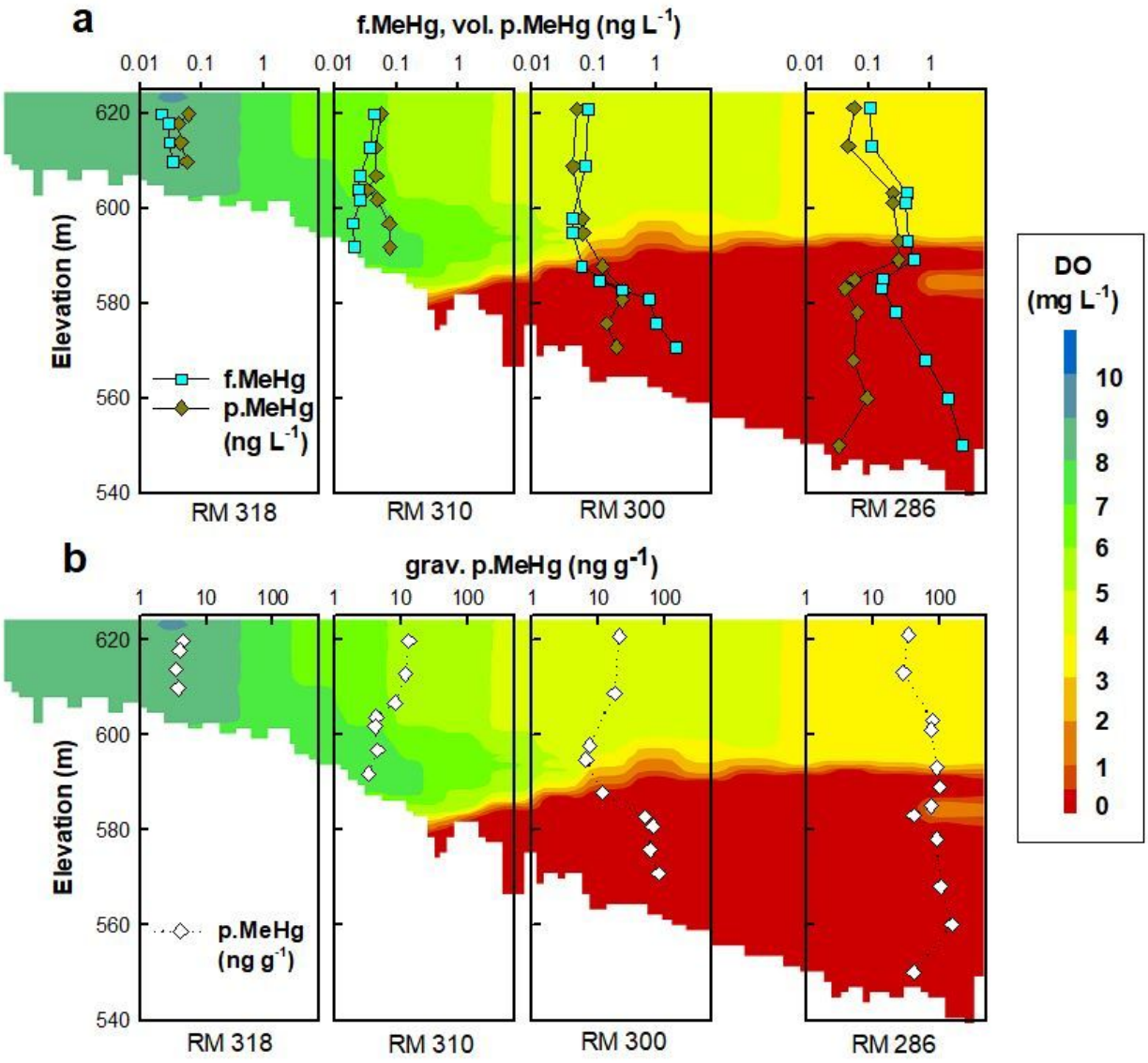

Figure 7. Depth profiles of (**a**) f.MeHg (ng L^{-1}) and volumetric p.MeHg (ng L^{-1}) and (**b**) gravimetric p.MeHg (ng g^{-1}) at river miles 318, 310, 300, and 286 in Brownlee Reservoir (9/25/2017) overlaid on a DO heat map (9/20/2017).[43] Plots show an increase in volumetric f.MeHg and p.MeHg (ng L^{-1}) with depth associated with hypoxic and anoxic water and the step-wise increase in gravimetric p.MeHg (ng g^{-1}) from upgradient to downgradient in the reservoir.

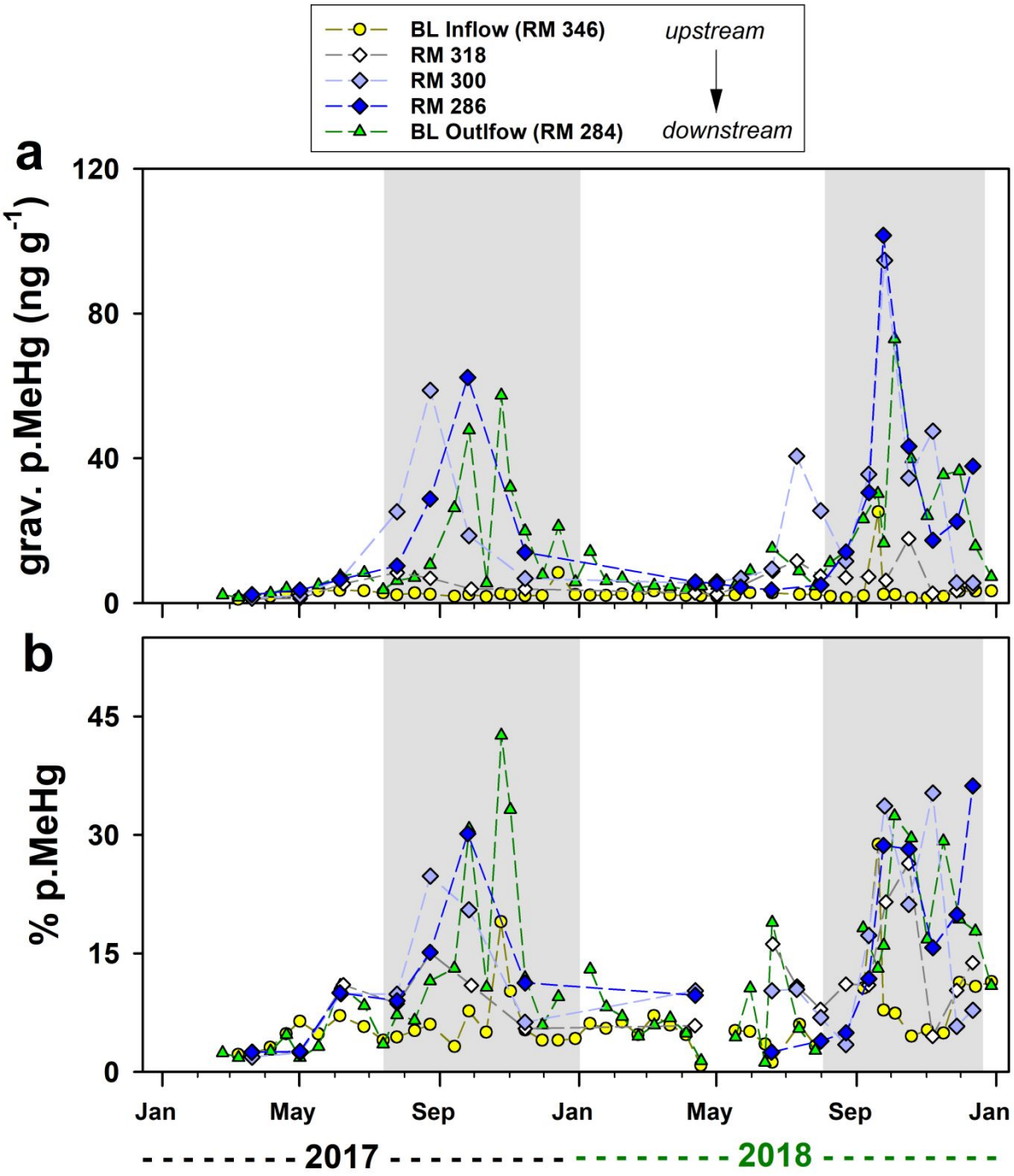

Figure 8. The volume-weighted (a) gravimetric particulate methylmercury concentration (p.MeHg, ng g^{-1}) and (b) percent particulate methylmercury (% p.MeHg) at the inflow and outflow of Brownlee Reservoir and within the reservoir at Snake River miles 318, 300, and 286 across 2017 – 2018.[43] The gray shaded areas identify the approximate timeframe of reservoir destratification (defined in Table S1). The volume-weighted data are summarized in Table S2.

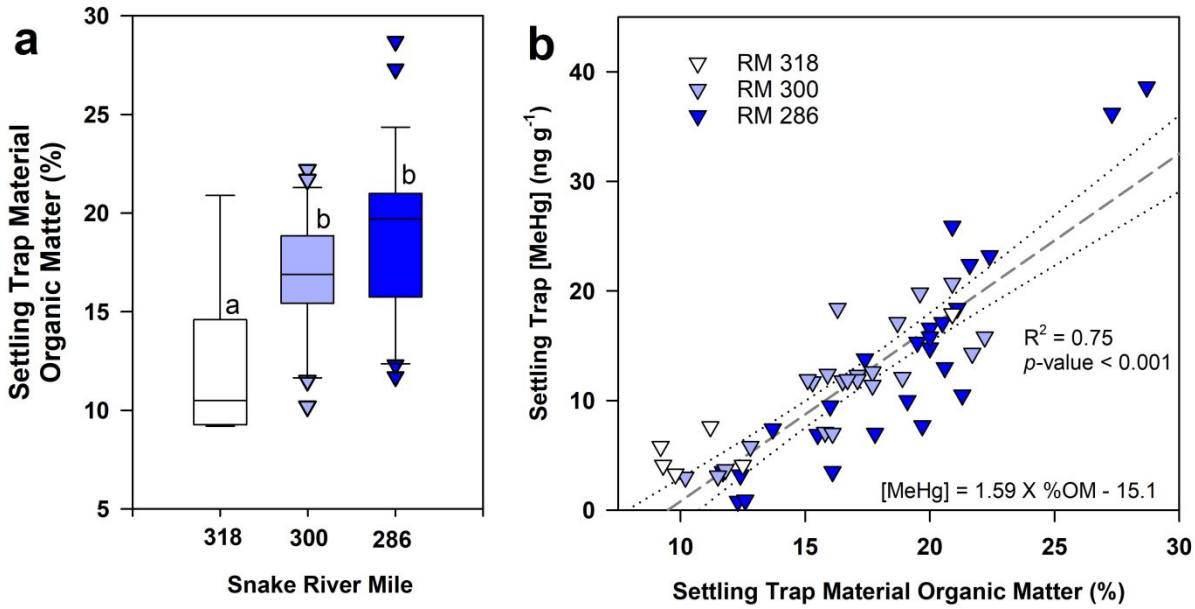

Figure 9. (**a**) Box and whisker plots of % organic matter (by loss on ignition) of settling particles collected in Brownlee Reservoir at river miles 318, 300, and 286 between 2017 and 2018 (<243 µm size); plots present the median and quartile range, error bars represent 10–90% percentiles, outliers are shown as data points, and letters designate statistical similarity and differences among comparisons (*t*-test).[43] (**b**) Scatter plot showing the significant linear correlation between the settling trap material MeHg concentration and organic matter content (n=53);[43] the gray dashed line is the linear fit of all data, and the black dotted lines are the 95% confidence intervals of the fit.